minerals

MDPI

Review

Origin of Banded Iron Formations: Links with Paleoclimate, Paleoenvironment, and Major Geological Processes

Jiangning Yin [1], Han Li [2,*] and Keyan Xiao [1]

[1] MLR Key Laboratory of Metallogeny and Mineral Assessment, Institute of Mineral Resources, CAGS, Beijing 100037, China; mark-johnson@163.com (J.Y.); keyanxiao1963@163.com (K.X.)
[2] Department of Law, Beijing Technology and Business University, Beijing 100048, China
* Correspondence: 20080502@btbu.edu.cn

Abstract: Banded iron-formations (BIFs) are marine chemical sedimentary rocks composed of siliceous and ferric materials, usually with typical thin layers or sheet structures. BIFs not only record a wealth of information about the state and evolution of the lithosphere, atmosphere, hydrosphere, and biosphere but also host the majority of the economic iron resources in the world. Here, we summarize the types, mineralogical, and geochemical characteristics of BIFs; analyze their formation conditions, their oxidative mechanism, and the absence causes of BIFs; and elucidate the associations between BIFs and major atmospheric oxidation events (Paleoproterozoic great oxidation event (2.4~2.1 Ga) and Neoproterozoic oxidation event (0.8~0.55 Ga)). BIFs are intimately associated with enhanced submarine magmatic–hydrothermal activities. Finally, it is concluded that the deposition and demise of BIFs are closely related to major geological events, and these major geological events interact with each other, jointly constraining the evolution of the atmospheric and marine environment and of geo-biological and geodynamic processes.

Keywords: banded iron formations; oxidation event; anoxic; major geological processes; paleoclimate; paleoenvironment; submarine hydrothermal fluid

Citation: Yin, J.; Li, H.; Xiao, K. Origin of Banded Iron Formations: Links with Paleoclimate, Paleoenvironment, and Major Geological Processes. *Minerals* **2023**, *13*, 547. https://doi.org/10.3390/min13040547

Academic Editors: Maxim Rudmin and Santanu Banerjee

Received: 27 February 2023
Revised: 7 April 2023
Accepted: 10 April 2023
Published: 13 April 2023

1. Introduction

Banded iron formations are unique iron-and silica-rich marine chemical sedimentary rocks deposited in mostly Archean and Paleoproterozoic strata in an anoxic marine environment. The term of BIFs originated from the description of iron formation in Lake Superior district [1]. BIFs are defined as chemical sedimentary rocks consisting of thin layers of siliceous bands (chert or its metamorphic products) alternating with iron-bearing minerals with an iron mass fraction usually 20%~35% and (SiO_2) 40%~50% [2]. BIFs have different names in different regions, such as banded ironstone in South America, quartz banded ore in Sweden, banded hematite quartzite in India, banded iron ore in South Africa, and magnetite quartzite in the Anshan-Benxi region of China. The distinguishable feature of BIFs is that they have obvious banded structures or rhythmic layers at both macroscopic and microscopic scales, and these bands have different widths, including the macro-bands (>2.54 cm), meso-bands (1.7 mm~2.54 cm), and micro-bands (0.3~1.7 mm) [3].

BIFs are distributed widely in all continents of the world. The earliest BIFs were formed at 3.8 Ga, such as Isua BIFs in Greenland and Nuvvaugittuq BIFs in Northern Qu' ebec; the latter were most likely formed at 4.3 Ga [4]. Precambrian BIFs were formed mainly in two periods: Archean to Paleoproterozoic (3.8~1.8 Ga) and Late Neoproterozoic (0.8~0.6 Ga) [3–6]. The peak of BIFs appeared at ~2.5 Ga, such as the BIFs in Hamersley Group in Australia and Transvaal BIFs in South Africa. Precambrian BIFs are components of the greenstone belt in ancient cratons, and most of them have generally been subjected to various grades of metamorphism, structural deformation, and dismemberment over a prolonged history of geological evolution [3]. The lack of modern analogs make the

reconstruction of the original depositional (basinal) setting of such BIFs very difficult [7]. The latest study suggests that ferrihydrite and partially oxidized or even purely ferrous greenalite are viable primary BIFs mineralogies [8]. Neoproterozoic BIFs occurred mainly in Phanerozoic orogenic belts, such as the Pan-African orogenic belt, the Brazil–African orogenic belt, and the Damar orogenic belts, also occurred in craton [5,9,10]. BIFs virtually disappeared from the geologic record at about 1.8 Ga and reappeared between 0.8 and 0.6 Ga [7], such as Rapitan BIFs in Canada and Urucum BIFs in Brazil. Mesoproterozoic BIFs are usually small in scale and volume [11–16]. Why BIFs are rare in the Mesoproterozoic is disputable. Recently, it is reported that a small number of Phanerozoic BIFs have been discovered successively [17,18], indicating the formation mechanism of these BIFs are still ambiguous.

Previous research suggests that the iron hosted in BIFs mainly comes from continental weathering [2,18] and marine hydrothermal fluid [7,19–21]. However, the oxidation mechanism remains controversial in terms of how the Fe^{2+} in seawater is oxidized to Fe^{3+} by microbial metabolism, cyanobacteria photosynthesis, and hypoxic photosynthesis [3,6,22,23]. BIFs are composed of oxide phases, carbonate phases, silicate phases, and sulfur compound phases [2], in which most minerals are not originally deposited but products of later diagenetic and metamorphic processes [7,23]. For example, the hematite is the product of dehydration of $Fe(OH)_3$ in early diagenetic processes [23], and the siderite may have originated from primitive inorganic precipitation [7,24] or microbial dissimilatory iron reduction (DIR) in the diagenetic process [25,26]. The origin of magnetite is more complex and may be formed in the process of diagenesis, metamorphism, and metasomatism.

The BIFs record a wealth of information on the evolution of the lithosphere, atmosphere, hydrosphere, and biosphere of the earth [18,27,28]. BIFs hold the key to understanding the biochemistry of the oceans and atmosphere and of how these interacted with microbial life prior to and during the evolution of oxygenic photosynthesis [26]. It is assumed that BIFs are linked to extreme climate changes, such as the great oxygenation event (GOE) [19,29,30]; the Neoproterozoic oxygenation event (NOE) [31–33]; the snowball earth event [7,34]; and major geological events, such as global mafic-ultramafic magmatism, juvenile continental and oceanic crust formation [34], volcanogenic massive sulphide formation (VMS) [35,36], mantle plumes, and large igneous provinces (LIP) [36,37]. Glikson et al., (2007) [38] observed the temporal consistency between the asteroid collision with the earth and the formation of BIFs and proposed that the formation of BIFs might be related to the asteroid collision with the Earth. He presents evidence for the succession of late Archaean impact event horizons—marked by microkrystite and microtektite-bearing ejecta/fallout units and associated turbidites and tsunami deposits—by ferruginous siltstone and banded iron formation. Impact units include the ~2.63 Ga Jeerinah Impact layer (JIL) and the ~2.56 Ga Spherule Marker Bed (SMB). The ~2.63 Ga JIL is directly overlain by debris flow boulder deposit, capped by a thin tuff unit directly overlain by the Marra Mamba iron formation [38].

In the past 100 years, extensive studies have been carried out on BIFs from different perspectives [39–49], which laid a solid foundation for studying the genesis of BIFs. Based on previous studies and the latest research results, the material sources, geochemical (isotopic) characteristics, genesis, and depositional environment of BIFs linked with major geological events, the paleoclimate, and the paleoenvironment were further studied and summarized in this paper.

2. Classification of Banded Iron Formations

Iron formations can be generally divided into BIFs and granular to oolitic granular iron formations (GIFs) [23]. GIFs formed at 2.9 Ga with a peak at around 1.88 Ga [49]. GIFs are very different from BIFs in texture as well as mineralogy (chert, iron oxide, iron carbonate, and silicate minerals). GIFs are characterized by recognizable detrital particles containing minor terrigenous particles with bands at a scale of tens of centimeters instead of millimeters as BIFs [7,50,51]. The cement of GIFs is usually iron oxide and carbonate

minerals. Flow structures (cross-bedding, ripple or scour marks) or sand-like structures are common in GIFs, suggesting that GIFs formed in shallow water near the continental shelf in or above the high energy environment, whereas BIFs mainly formed in the deep sea (>200 m) [45]. Both BIFs and GIFs were formed during the rising of the sea level [3].

Precambrian BIFs can be divided into Algoma-type and Superior-type based on their paleodepositional environment and associated rock types [1]. Algoma-type BIFs are typically associated with greywacke, fine-grained volcanic (clastic) rocks in the middle and upper part of the Archean greenstone belt and spatially adjacent to turbidite assemblages [52,53]. Tectonically, the Algoma-type BIFs mostly occurred in intracraton rifts or volcanic arcs settings adjacent to eruptive centers, similar to the closed basin of the Red Sea [54]. The BIFs in Archean greenstone belt in western Greenland and Yilgarn craton in Western Australia are the most significant Algoma deposits in the world [7,55]. Most of the BIFs in north China craton belong to the Algoma type. By comparison, Superior-type BIFs were deposited in near-shore continental environments within the passive continental margin and distal from submarine volcanic emanations in the Neoarchean and Paleoproterozoic [56]. Superior-type BIFs were significantly associated with sedimentary formations, such as carbonate rocks, quartz sandstones, black shales and minor amounts of other volcanic rocks with granular or oolitic structures. Some Superior-type BIFs may developed to be GIFs. Hamersley BIFs of Western Australia and Kuruman BIFs in South Africa belong to typical Superior type. Algoma-type BIFs are typically highly deformed and metamorphosed, forming narrow lenticular and discontinuous outcrops associated with pillow lavas and greywacke, whereas the Superior-type BIFs are typically relatively unmetamorphosed and undeformed, with a widespread continuous outcrop, and are associated with conglomerate, quartzite, and stromatolitic carbonate rocks [7]. Positive Eu (europium) anomalies indicate a hydrothermal source for the deposition of iron. Hydrothermal fluids commonly display pronounced positive Eu anomalies [57–59]. Algoma-type BIFs are characterized by much larger Eu anomalies (>1.8) than Superior-type BIFs (<1.8), indicating the former were incorporated with more components of volcanic-related hydrothermal emissions. The lower Eu anomalies of Superior-type BIFs suggest less input of volcanic-related hydrothermal emanations and the further addition of other sources, including terriginous sediments and seawater. In this respect, the BIFs record the signatures of the paleoenvironment transformation and chemistry of Precambrian oceans.

Cherty BIFs deposited in the Neoproterozoic is classed as Rapitan (or Cryogenian) type [60]. The Rapitan-type BIFs mainly occurred in the glacial age in Neoproterozoic and mostly hosted in glaciogenic lithologies such as diamictites and dropstone layers [55,61,62] overlaid by giant thick carbonate rocks (e.g., Urucum BIFs [63]). The Rapitan-type BIFs usually occurred in the rifted basin in the interior or at the edge of the Rodinian supercontinental. Superior-type BIFs contain more hematite and less magnetite than Algoma-type BIFs with predominant quartz gangue and minor amphibole and chlorite. In comparison, the main ore minerals of the Rapitan-type BIFs are magnetite [9]. A detailed comparison of the three BIFs types can be found in Table 1.

BIFs are important as the major source of the iron ore industry, but BIFs themselves do not represent iron ore in economic senses unless BIFs are upgraded to iron ores through complex geochemical processes, such as hydrothermal enrichment (<5 million years), or weathering enrichment (which often took place during the last 20 million years [54]). BIF-hosted iron constitutes the world's largest and most high-grade iron deposits, accounting for >60% of the world's iron resources [9]. Despite the large number of Algoma BIFs iron occurrences, Superior-type BIFs are far more important than other types of BIFs worldwide in terms of economic value and volumes [39] (Figure 1). For example, some Superior-type iron ores have an area of more than 10^5 km^2 with hundreds meters of ore thickness, containing more than 10^{13} tons of iron resources. Algoma-type BIFs are relatively small in scale, with an area generally less than 100 km^2 and ore thickness rarely exceeding 50 m, and resource quantity is generally less than 10 billion tons [41]. Rapitan-type BIFs have

even less volume, with an area of no more than 10 km^2, and the thickness of single ore layer is generally no more than 10 m [5].

Table 1. Comparison of the three BIFs types.

BIFs Types	Formation Age	Tectonic Settings	Rock Assemblages	Significant Deposits/Regions
Algoma	Archean and Paleoproterozoic	Intracraton rifts or volcanic arcs settings	Greywacke, fine-grained volcanic (clastic) rocks	Archean Yilgarn and Pilbara deposits
Superior	Neoarchean and Paleoproterozoic	Passive continental margin	Sedimentary formations, such as carbonate rocks, quartz sandstones, and black shales	Hamersley and the Transvaal deposits in Australia and South Africa
Rapitan	Early Neoproterozoic	Rifted basin	Glaciogenic lithologies such as diamictites and dropstone layers	Urucum in the Mato Grosso State, Brazil, and Rapitan in the Northwest Territories of Canada

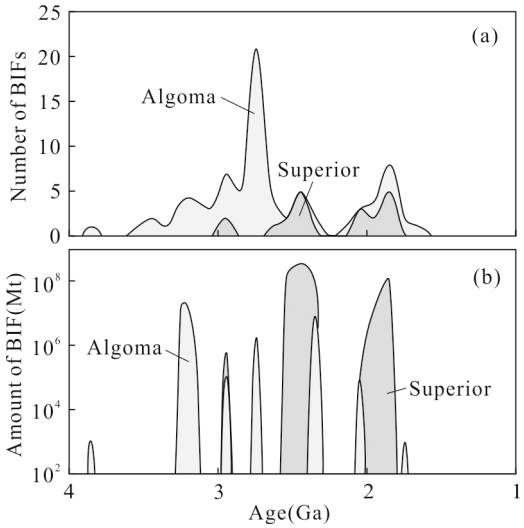

Figure 1. Comparison diagram in the number (**a**) and abundances (**b**) of Algoma-type and Superior-type BIFs through time (modified after Huston et al., 2004).

3. Formation Conditions of BIFs

The classical and most widely accepted model for Fe formation deposition invokes ambient free oxygen (O_2)-induced ferrous Fe oxygenation. This model, championed by Cloud [64] (Cloud, 1965), suggests that deposition of Fe formation occurred at the interface between oxygenated shallow waters and upwelling Fe-rich reduced waters. The oxidizing shallow waters have been linked to prolific communities of oxygenic photosynthesizers [19,64,65]. It is supposed that three basic conditions are required for the vast deposition of iron in the ocean [3,20]: (1) reducing atmospheres or atmospheres with lower oxygen fugacity [66]; (2) sulfate and low sulfide concentrations [67]; and (3) high temperature hydrothermal fluids [7]. Cox et al., (2013) [6] proposed that there were three conditions for the formation of Neoproterozoic BIFs: (1) Anoxic seawater keeps Fe^{2+} soluble, which is favorable for the accumulation and deposition of iron. The concentration of iron in modern seawater is very low, and its retention time is short, about 1 to 100 years.

Iron is highly soluble and has a long retention time in anoxic and sulfate-poor environments, such as the Archean ocean [68,69]. (2) The hydrogen sulfide to ferrous iron ratio is less than 2 ($H_2S/Fe^{2+} < 2$). If $H_2S/Fe^{2+} > 2$, Fe^{2+} is efficiently converted to pyrite and the concentration of dissolved iron in seawater decreases. Therefore, the seawater constitute an anoxic and iron-rich environment ($H_2S/Fe^{2+} < 2$) rather than an anoxic and sulfide environment [6]. (3) The oxidation mechanism functions, i.e., the formation of $Fe(OH)_3$ by biological or abiotic oxidation processes from large amounts of dissolved Fe^{2+} in seawater occurs [3]. Based on a previous study and in combination with the latest research, we conclude that the formation of BIFs requires the following three conditions: (1) a substantial marine iron reservoir; (2) a reduction in the water environment, although the whole water does not need to be reduced; (3) that the Fe^{2+} precipitation mechanism functions, i.e., Fe^{2+} precipitation to form the original $Fe(OH)_3$.

3.1. Material Sources

The sources of iron in BIFs are controversial. Previous studies suggested that the iron was derived from the weathering of terrigenous materials [2,19], whereas the iron in volcanogenic BIFs may be directly derived from submarine volcanic activities [7]. It is known that there are two iron sources in the modern global ocean: terrigenous input and submarine hydrothermal input. Terrigenous input includes rivers, aeolian dust, glaciers, and coastal erosion [70]. The basalt–andesite–rhyolite formed by marine volcanism is predominant in the Archean ocean, and consequently the volcanogenic materials have dominated the marine solute input [71]. In addition, the higher geothermal gradient (>60 °C/km) in the Archean promotes the strong free convection of seawater, thus forming the submarine hydrothermal system dominated by volcanic materials, which is the main source of iron [7].

Due to the minimal involvement of organic C (carbon) in the BIF deposition, there is no evidence to support the claim that BIF deposition is directly related to microbial activities. Klein (2005) held that Fe and Si were inorganic products of weathering of continental margin rocks [7]. This model represents the sedimentary environment of Neoarchean-Paleoproterozoic BIFs [7] but mainly in the Paleoproterozoic [72]. However, many other studies have suggested that biological processes are involved in BIF deposition [72–74], such as shallow-water carbonate-shale lithology in BIFs (rich in organic carbon), microbial dissimilated reduction by phosphorus, and Fe^{3+} hydroxides near the continental shelf.

Although there is no consensus on the sources of iron in BIFs, the general accepted view is that the iron comes from two sources, namely, continental weathering [2,19] and submarine hydrothermal activities [7,20], or a combination of both processes [72].

3.1.1. Submarine Hydrothermal Sources

Previous studies indicated that BIFs and hydrothermal fluids that originated from the mid-ocean ridge shared similar REE characteristics (such as positive Eu anomaly), and it was speculated that the iron mainly came from the submarine hydrothermal vents [7,75]. Saito et al., (2013) [76] supported the view by direct observations of iron-containing hydrothermal fluids from mid-ocean ridges. Nd isotopes can be used to trace the origin of iron in BIFs [77,78]. Generally, hydrothermal fluids display high Sm/Nd ratios and positive Nd isotope values similar to mantle source materials, whereas continental materials usually show crustal characteristics with low Sm/Nd ratios and negative Nd isotope values. Nd isotopes of modern seawater are similar to those of river water and atmospheric dust, reflecting the addition of terrigenous detrital materials [77]. Alexander et al., (2009) [79] demonstrated that BIFs older than 2.7 Ga usually have relatively uniform εNd(t) (Nd model age) values ranging from +1 to +2, which is a typical Nd isotope characteristic of deep seawater dominated by submarine hydrothermal fluids [77]. Almost all submarine hydrothermal activities occur at plate boundaries owing to the close coexistence of magmatic activity, seismic activity, and high-temperature hydrothermal fluids temporally and spatially. Submarine thermal springs mainly occur in modern mid-ocean ridges, back-arc

basins, and submarine volcanic island arcs [80]. Therefore, a commonly held view is that the tectonic environment such as the mid-ocean ridge is the main source area of iron in the Precambrian BIFs [81].

Modern hydrothermal vents at mid-ocean ridges vary in iron content, and Isley (1995) [82] estimated that modern submarine hydrothermal vents provide about 0.01 Gt (billion tons) of iron per year. Due to the lack of sulfate in the circulating seawater and the low oxygen or anoxic environment, the molar concentration of iron in the hydrothermal fluid can be as high as 80 mmoL/kg [81]. The molality of iron in hydrothermal fluids in the modern island arc or back-arc basins can also be as high as 2500 mmoL/kg [81]. Johnson et al., (2019) [21] believed that pre-GOE hydrothermal fluids could form 0.134 Gt of iron per year, indicating that Archean submarine hydrothermal fluids are crucial for Fe^{2+} enrichment in seawater. Additionally, the iron content of Archean shales is significantly higher than that of Phanerozoic shales, suggesting higher iron content in sedimentary water. Extensive studies have shown that these submarine hydrothermal solutions are mainly the result of water–rock exchange reactions between circulating seawater and oceanic crust (mafic and ultramafic rocks). Iron and silica leached from igneous and volcanic rocks by hydrothermal fluids [80] is precipitated on contact with seawater; thus, iron-rich sediments accumulated and deposited around the vents [14,83].

3.1.2. Terrigenous Sources

The iron input from rivers contributes most of the iron sources to the modern ocean as a colloid or dissolved state. The surface of the colloid is charged, which is controlled by the charge difference between the river and the sea. Most of the iron input by the river precipitates quickly on the continental shelf and cannot effectively participate in the marine iron cycle [84]. In the early diagenetic process, iron is activated and re-migrated under the influence of the transformation of the redox environment in the pore water of sediments or the upper water, which is a very important part of the marine iron cycle [85]. Previous studies on Nd isotopes of BIFs show that εNd(t) values of BIFs are mostly between the depleted mantle and the continental crust (Figure 2), suggesting that seawater may be an important source of iron for BIFs. εNd(t) values of some BIFs are as low as −10, indicating the addition of ancient materials.

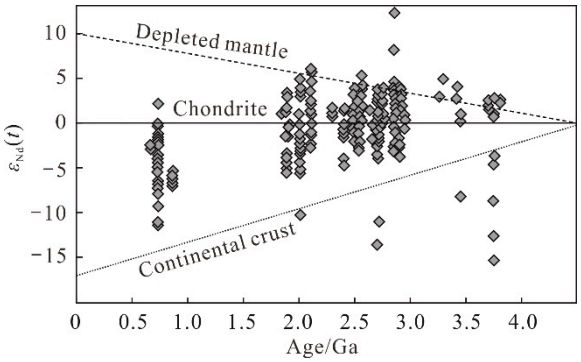

Figure 2. Summary of εNd(t) isotope data of BIFs through Earth's history. Data of εNd(t) values of BIF is from [86–91].

Based on Nd and Fe isotope data and REE characteristics of sedimentary sequences in Dales Gorger, Hamersley Basin, Western Australia, during the period of 2.50~2.45 Ga, Li et al., (2015) [76] summarizes the two-source model of the origin of BIFs. Some BIFs have high εNd and negative δ^{56}Fe values, indicating hydrothermal end-member components, while the relatively low εNd and δ^{56}Fe values reflect the contribution of continental materials, which are transported to deep-basin sediments through iron migration by microorganisms under reducing conditions. Except the abiogenic Fe from extensive shallow marine hydrothermal sources, biogenic Fe is also an important source, and the proportion

of the two sources varies with the scale and time of basin water cycle. It is generally accepted that the sources of iron come from both seawater and volcanic materials. The study by Smith et al., (2013) [92] on the sedimentary model of Witwatersrand BIFs in Archean shows that, during the primary period of BIFs sedimentation, iron was supplied mainly by submarine hydrothermal fluid in the ocean basin far away from the continent. If it was proximal to the ancient continent, terrigenous detritus was added. However, in the deep ocean basins from Archaean to Paleoproterozoic, the addition of terrigenous materials may be insignificant [3,73].

Similar to the source of iron, it is recognized that silicon in BIFs is derived from both submarine hydrothermal fluid and continental physical weathering [3]. Based on the study of silicon isotope, it can be inferred that silicon and iron have the same sources, mainly from submarine hydrothermal fluids. According to the different Nd isotopic compositions and Ge/Si ratios between seafloor hydrothermal fluid and terrigenous materials [93], it is proposed that the sources of silicon and iron are decoupled [93,94], namely, iron comes mostly from submarine hydrothermal fluids, whereas silicon comes mostly from the continents material weathering. The adsorption precipitation of silicon with ferric hydroxide [95] or silica precipitation [96] can result in a strong fractionation of Ge/Si ratio. In addition, Ge may be released by pore water during diagenetic process, which also affects the Ge/Si ratio [96].

3.2. Anoxic Marine Environment

Oxygen plays a crucial role in the evolution of ecosystems and is strongly associated with the survival of the vast majority of life on Earth. The oxygen content in the modern atmosphere is about 21%, and previous studies show that the atmosphere mainly experiences two oxidation events, namely, the Paleoproterozoic GOE and NOE. The BIFs record the chemical composition and redox state of the ancient oceans. The abundance of BIFs in the early Precambrian indicated the prevalence of anoxic, iron-rich oceans [97]. Ce has two valence states (Ce^{3+} and Ce^{4+}) and is widely used as a redox indicator for sedimentary basin seawater due to its sensitivity to redox environment [6,20]. In most Precambrian BIFs, no obvious negative Ce anomaly was observed, indicating that the BIFs were mainly formed in the hypoxic environment [6]. In oxidized seawater, the iron retention time is short and its concentration is low, whereas in an anoxic environment, the iron retention time is long and biological or abiotic oxidation would trigger iron precipitation, which displays significant iron isotope fractionation [72]. Significant fractionation of iron isotopes can be observed in most Precambrian BIFs, indicating the partial oxidation of iron in a hypoxic or anoxic sedimentary environment [69,98]. The modern ocean has a very low iron concentration of only 0.6 nmol/L [99,100]. The concentration of iron in the Proterozoic ocean was 50 μmol/L [70], whereas the solubility of iron before GOE was higher and reached 100 μmol/L in the Archean ocean [101], which triggered the vast accumulation and precipitation of dissolved ferrous iron. Although BIFs were mainly formed in the early Precambrian, the oceanic redox environment of early Precambrian dynamically fluctuated [39]. Holland (1984) [70] suggested that the Neoproterozoic deep sea redeveloped from the high-oxygen fugacity to the medium reducing environment, while Canfield (1998) [102] asserted that the Neoproterozoic deep sea changed from the highly reducing condition to the medium reducing condition and that the deep sea was an iron-rich environment. In conclusion, the deposition of BIFs do not require the entire seawater anoxia.

3.3. Oxidation Mechanism

The deposition of BIFs spans major processes in the early evolution of the Earth, from early CO_2 and CH_4-dominated atmosphere to a CO_2-rich atmosphere [30], suggesting that Precambrian BIFs can be formed through different oxidation mechanisms. The primary process of BIFs precipitation causes the dissolved Fe^{2+} in seawater to be oxidized to form Fe^{3+}. Bekker et al., (2010) [3] concluded that the dissolved Fe^{2+} in the ocean is oxidized to form BIFs in the following three ways.

(1) Fe^{2+} was oxidized by oxygen produced by cyanobacteria: the traditional view is that the oxygen in the Archean oceans mainly came from the photosynthesis of cyanobacteria. Substantial evidence supports that there were no eukaryotes prior to 1.9 Ga based on the fossil record [103]; cyanobacteria were the most important photosynthetic oxygen releasers in Archean oceans. Fe^{2+} reacts with oxygen as follows:

$$2Fe^{2+} + 0.5O_2 + 5H_2O \longleftrightarrow 2Fe(OH)_3 + 4H^+ \quad (1)$$

The date of the earliest emergence of photosynthesis is controversial. Frei et al., (2009) [104] found that Cr isotope fractionation could be observed in BIFs during 2.8~2.6 Ga, suggesting that ocean oxidation began during this period. However, according to latest studies by Cardona (2019) [105], a homodimeric photosystem with sufficient oxidizing power to split water had already appeared in the early Archean about a billion years before the most recent common ancestor of all of the described Cyanobacteria capable of oxygenic photosynthesis, and well before the diversification of some of the known groups of anoxygenic photosynthetic bacteria [106]. Recently, biological evidence has supported the view that early forms of oxygenic photosynthesis were present throughout the Archean eon and oxygenic photosynthesis was already well established by 3.0 Ba (billion years ago), reconciling geochemical and molecular evolution evidence bases [106]. Hoashi et al., (2009) [103] found that the hematite in jasper of Pilbara craton in Australia was formed by the oxidation of Fe^{2+} in the original seawater and claimed that oxidation had begun before 3.46 Ga in the middle-deep sea. Kendall et al., (2010) [106] studied the black shale of the Campbellrand–Malmani carbonate platform in South Africa during 2.5–2.6 Ga and found that it was rich in Re and low in Mo. Combined with the study of iron components, he assumed that oxidation was common in the Archaean marginal sea, but the deep ocean was still anoxic. Regardless of the anoxia in the Archean atmosphere, oxygen may be present as "oases" in the ocean [107]. Some researchers proposed that the ocean has already been redox-stratified in this period, producing an oxygenated upper layer in the ocean. Recently, based on carbon isotope stratigraphy of Precambrian iron formations, Tsikos et al. proposed abiotic and anoxic models for BIFs genesis prior to GOE [108]. In conclusion, the oxygen in the ocean was variable and fluctuated dynamically during this period, but the occurrence date, content, and distribution style of oxygen in the ocean are disputable.

(2) Fe^{2+} oxidation caused by bacterial metabolism: a large amount of iron bacteria (such as ciliated bacteria and trichoderma bacteria) has been found in modern iron-rich groundwater and streams. It can be speculated that such micro-aerobic microbial oxidation also plays an important role in the formation of BIFs [3]. Iron-oxidizing bacteria, oxygen, carbon dioxide, and water produce the following reaction:

$$6Fe^{2+} + 0.5O_2 + CO_2 + 16H_2O \longleftrightarrow [CH_2O] + 6Fe(OH)_3 + 12H^+ \quad (2)$$

In addition, Ehrenreich et al., (1994) [109] proposed the following anoxia photosynthetic oxidation process:

$$4Fe^{2+} + 11H_2O + CO_2 \longleftrightarrow [CH_2O] + 4Fe(OH)_3 + 8H^+ \quad (3)$$

Experimental studies proved that these phototropic bacteria can promote the oxidation of Fe^{2+} to Fe^{3+}, thus causing the rapid deposition of BIFs [110,111]. In the Archean ocean, light could effectively oxidize Fe^{2+} to Fe^{3+} at depths of several hundred meters, allowing light to easily oxidize most of the $Fe^{2+,}$ which rose with the hydrothermal flow even before it rose to the overlying oxide layer [3,111]. Siderite is the dominant mineral in Xiamaling BIFs formation, North China Craton. Canfield et al., (2018) [112] presumed that Fe^{2+} of the siderite was oxidized mainly through anoxic photosynthesis.

(3) Cairns-Smith (1978) [113] proposed that Fe^{2+} could be photochemically oxidized by UV (ultraviolet light) before the appearance of atmospheric oxygen, and this reaction could easily occur in acidic water with UV wavelength of 200~300 nm:

$$2F^{2+}{}_{aq} + 2H^{+} + hv \rightarrow 2Fe^{3+}{}_{aq} + H_2 \quad (4)$$

where *hv* stands for high energy sunlight (200–400 m) and aq denotes acquirement. Cox et al., (2013) [6] summarized the above processes as abiotic oxidation processes and biological oxidation processes. Abiotic oxidation processes include the first and third processes mentioned above, whereas the second is a biological process. Furthermore, abiotic processes include the reaction of Fe^{2+} with free oxygen in seawater, which may be mainly involved in the precipitation of Neoproterozoic BIFs. Since oxygen concentration in Neoproterozoic seawater has reached a certain content, Fe^{2+} oxidation in Neoproterozoic seawater may have occurred through the exchange of oxygen between seawater and atmosphere as well as the addition of oxygen-rich glacial meltwater during the interglacial period [114,115]. Recently, Thibon et al., (2019) [100] proposed another abiotic oxidation process of early Precambrian BIFs. They found that from 2521 Ma to 2394 Ma, the marine iron retention time was increased from 0.2 Ma to 2.3 Ma, that is, the concentration of iron in seawater increased from 6.4 mm/kg to 37 mm/kg, and the electron acceptor of Fe^{2+} oxidation was considered to be CO_2 (or dissolved inorganic carbon converted into CH_4), leading to the enrichment of CH_4 in the ocean. The latest experimental simulations show the spontaneous oxidation of ferrous hydroxide to ferric iron. The finding suggests that anoxic iron oxidation may have contributed to the formation of oxide-facies BIFs, especially Algoma-type BIFs that likely formed in semi-restricted basins where ferrous hydroxide saturation was more easily achieved. The decomposition of ferrous hydroxide and related green rust formation is one mechanism to explain the occurrence of ferric iron in Archean BIFs. These observations and the wide range of depositional settings of BIFs highlight the necessity to recognize the potential involvement of multiple mechanisms in the genesis of BIFs, and that it is likely no single process can explain all known BIFs [113].

4. The Deposition and Demise of the BIFs

4.1. Early Precambrian BIFs

Substantial evidence supports the claim that the Earth's ancient atmosphere was anoxic in the Precambrian period, such as the sulfur isotope nonmass fractionation equilibrium [33,116,117]; the ratios of iron, molybdenum, and carbon isotopes in sediments [118]; the absence of a red layer; and the Fe^{2+}-dominant leaching products in paleosoils [119]. There are various opinions on the mechanism of early Precambrian BIFs regarding submarine hydrothermal venting. Based on the studies of modern ocean sediments, there are two main points: (a) Ocean upwelling current: the BIF sedimentary site is relatively independent from the seawater from which its material originates [120], and the hydrothermal minerals are brought to shallow sea or craton margin deposition through the upwelling of ocean current [73]. (b) Convection and circulation of seawater: hot fluids, consisting of marine and connate water leaching iron, silica, and other elements from mafic and ultramafic rocks associated with mantle plumes or mid-oceanic ridges and active spreading centers are released into the ocean at underwater hot springs (black smokers). On contact with cold marine water, the least soluble elements are precipitated in the form of colloidal hydrous silicates (clay minerals) and hydroxides close to the hydrothermal vent. The hydrothermal fluids are high in silica and low in alumina, causing the precipitation of alumina-poor iron silicates (nontronite) that dissociate into iron hydroxide and amorphous silica during diagenesis. The amorphous silica is typically entrapped by iron oxide laminae to form bands of chert. Breaches of the iron oxide laminae permitted the escape of the gelatinous amorphous silica during compaction and dewatering, leaving a chert-free residue as the protore of non-hydrothermal sedimentary high-grade iron ore [86,121,122]. Smith et al., (2013) [92] studied the BIFs of the ancient West Rand in South Africa and found that the sedimentary sequences were hematite–magnetite associations, magnetite–siderite and siderite from bottom to top, indicating that hematite–magnetite associations were deposited at the farthest end of the basin, while magnetite–carbonate and mudstone were deposited near the coast. The West Rand BIFs was formed during the maximum marine

transgression, when the deep hydrothermal fluid surged up below the upper transmittance zone and in turn would trigger BIF deposition. Fe-oxidizing bacteria produce limited oxygen at the interface between the hydrothermal column and the surrounding seawater, and Fe^{2+} is oxidized to form the original $Fe(OH)_3$, which either precipitates on the seafloor or was reduced to ferric ion by the action of the hydrothermal column. At the far shore end, the ferric hydroxide was converted to hematite during the later diagenetic compaction process and was preserved. Magnetite was formed when hydrothermal columns came into contact with seafloor sediments; by the nearshore side, $Fe(OH)_3$ is transformed into Fe-rich carbonate minerals with the addition of organic carbon, and in the nearshore shelf, Fe-rich aluminosilicate minerals were formed with the increasing contribution of terrigenous detrital materials significantly. Above the hydrothermal columns, some iron-poor detrital deposits occurred. Accordingly, the following BIFs sedimentary model could be established (Figure 3). This model reflects the changes of hematite–magnetite BIFs from the lowest and furthest part of the basin to the top and near the coast, from magnetite–siderite to siderite BIFs of carbonate facies, then to iron mudstone, iron mudstone siltstone, and finally to continental sandstone. At a certain depth of the basin, due to neutral buoyancy [87], the deep reduction in iron-rich hydrothermal liquid upwelled below the upper photic zone, resulting in hematite–magnetite BIF deposition. In the distal part of the basin, where the base of the plume was not contact with the sediment and siliciclastic input was minimal, the ferric oxyhydroxides would be transformed to and preserved as hematite in hematite-bearing iron formation. Where the plume was in contact with the sediment and organic carbon input was limited, the ferric oxyhydroxides would be transformed to magnetite by the Fe^{2+} in the plume in a nonredox reaction, as proposed by Ohmoto (2003) [123], and magnetite-bearing iron formation would be preserved. Closer to the coast, where the plume was in contact with the sediment and organic carbon input was higher, but still with limited siliciclastic input from the coast, the oxidation of organic carbon through the reduction in hematite would have led to the formation of siderite and/or ankerite along with magnetite formed by iron respiration in the presence of organic matter and/or the addition of dissolved Fe^{2+} from plume water. Above the top of the hydrothermal plume in the shallower, more proximal parts of the basin, there was very little iron input into the sediment, and only iron-poor mudstone, siltstone, and sandstone were preserved.

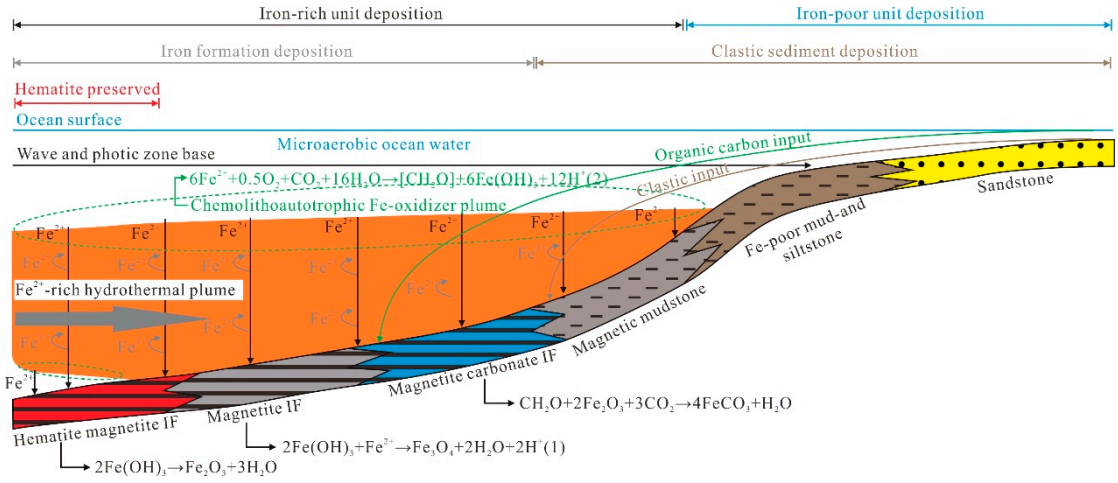

Figure 3. Depositional model of early Precambrian BIFs (modified after [92]).

Most early Precambrian BIFs have undergone varying degrees of metamorphism. For example, the BIFs in Hamersley of Western Australia and the BIFs in Kaapvaal of South Africa experienced low-grade metamorphism (sub-greenschist-greenschist facies), and the silicate minerals in the low-grade BIFs mainly include iron serpentine, minnesotaite, iron amphibolite, and stilpnomelane [7]. The early Archean BIFs in southern West Greenland experienced amphibolite facies to granulite facies metamorphism [124], the

Ananben area of China experienced greenschist facies to amphibolite facies metamorphism, and the eastern Hebei of China experienced greenschist facies to granulite facies metamorphism [46,125]. Under intermediate metamorphism, iron carbonate minerals, quartz, and minnesotaite will form ferricite and ferricite; the recrystallization of magnetite and hematite will occur, and the particle size will become coarser. In some areas, there may also be ferroaluminite. Anhydrous silicate minerals will be present in high-degree metamorphism. Carbonate minerals (dolomite and calcite) occur in both low- and high-grade metamorphism. Figure 4 lists the stable mineral assemblages in different grades of metamorphism. All of the metamorphic reactions are essentially isochemical, except for prevalent dehydration and decarbonation [7].

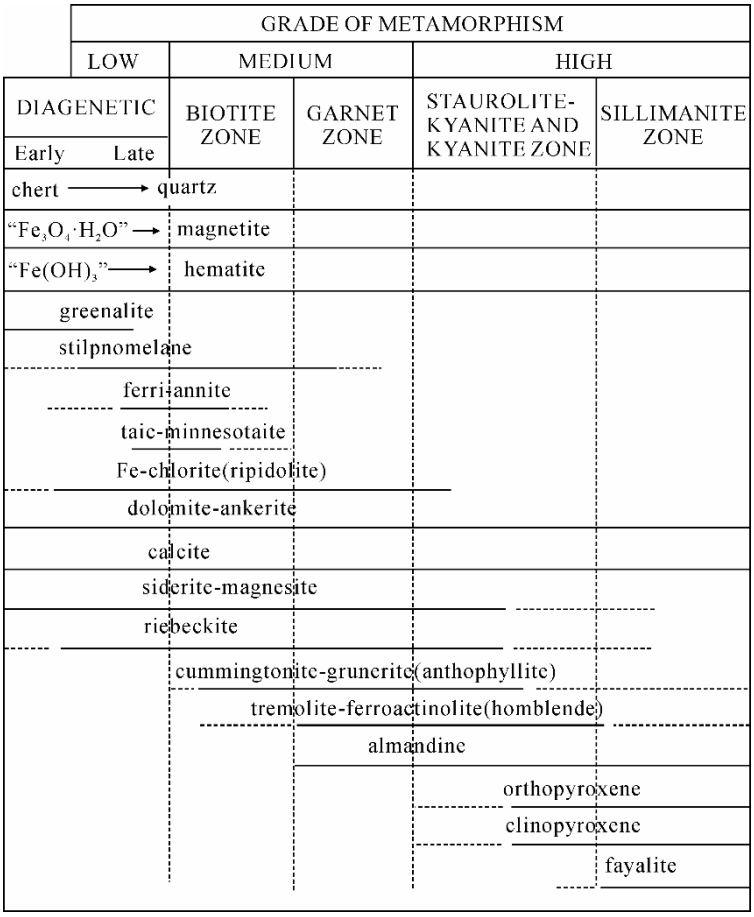

Figure 4. Relative stabilities of minerals in metamorphosed BIF (modified after [7]). Full line express common stability field, and dashed line express possible stabilities of minerals.

4.2. The Demise of the BIFs in the Mesoproterozoic

It has long been known that BIF absence occurred in the Mesoproterozoic (1.8~0.8 Ga) [7,14,39]. The following explanations exist for the absence of BIFs in the Mesoproterozoic: the ocean was completely oxidized in the Mesoproterozoic (Figure 5a). Consequently, Fe^{2+} was oxidized from submarine hydrothermal solutions, resulting in the colloidal precipitation of ferric hydroxide and the depletion of iron in dilution, which is not favorable for the formation of BIFs [70]. Canfield (1998) [104] argued that although BIF deposition ended in the Mesoproterozoic, the deep sea was still anoxic and sulphurized, where iron was precipitated in the form of sulfide, thus reducing the dissolved iron in seawater and preventing the formation of BIFs (Figure 5a). Lascelles (2013) holds that plate subduction destroyed the formation and preservation of BIFs. Although the commonly held view is that the deep ocean was anoxic in the Mesoproterozoic, Lascelles does not agree that the

deep ocean was vulcanized. Recently, based on the studies of the C-S-Fe system, the Mo isotope, and iron components, it can be deduced that the deep ocean in the Mesoproterozoic was similar to the Archaean ocean, both of which were anoxic and iron-rich environments, and the vulcanized environment only existed locally at the continental margin [126–128]. Planavsky et al., (2011) [126] argued that the formation of BIFs was related to the continuous supply of iron by strong submarine hydrothermal plume and the long-term iron-rich environment, and that the absence of BIFs in the Mesoproterozoic might be due to waning volcanic magmatism and diminished marine hydrothermal activities.

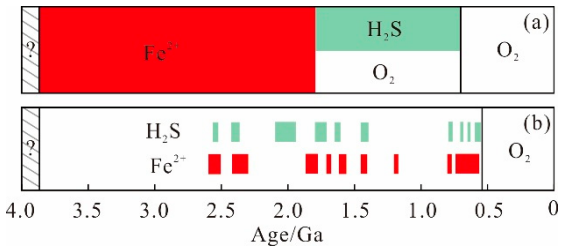

Figure 5. Evolution of Earth's marine conditions through time (modified after [126]). (**a**). Classical models of the chemical composition of the deep ocean. (**b**) Distribution of Precambrian euxinic and ferruginous deep waters, based on the shale record.

The shales recorded the anoxic and iron-rich marine environment in Mesoproterozoic (Figure 5b). Some scholars believed that the early Mesoproterozoic ocean was an anoxic and iron-rich environment, and it was not until the emergence of multicellular eukaryotes in 1570 Ma that the ocean began to oxidize [129], while Shang et al., (2019) [130] found that the oxidation was only the pulsating oxidation of seawater. Admittedly, the eukaryogenesis is a contentious issue and there is not full consensus yet [131]. Planavsky et al., (2018) [132] suggested that there were multiple periods of ocean oxidation in the Mesoproterozoic. Although large BIFs were not pervasive during this period, some small BIFs were present. In addition, BIFs associated with VMS and SEDEX (sedimentary exhalative) deposits occurred, such as BIFs in Broken Hill [11,14], BIFs in the Pecos greenstone belt in New Mexico [12], and BIFs in the western North Qilian mountain in China in the Mesoproterozoic [16,43]. These BIFs may have recorded the oceanic atmosphere at the time. Previous studies on BIFs associated with VMS in central Arizona and New Mexico in the United States at 17 Ga suggested that the BIFs were formed in oxidized deep-sea environment [133]. Canfield et al., (2018) [116] found that Xiamaling Formation in the North China Craton in 14 Ga was composed of siderite-rich iron, which was formed in an anoxic environment. The Jingtieshan BIFs in the western part of North Qilian in China were formed in the redox stratified and iron-rich ocean with surface oxidation and deep hypoxia environment [16,24]. In conclusion, the mass disappearance of BIFs reflects the dramatic changes in the redox state and chemical composition of the ocean from 1.8 Ga.

4.3. Neoproterozoic BIFs

Ilyin (2009) [5] believed that the exact formation age of Neoproterozoic BIF should be 0.85~0.63 Ga, when atmospheric oxygen had reached a very high level [106], which was different from the low atmospheric oxygen content during the formation of early Precambrian BIFs and the oxygen deficiency environment in the deep sea [33,106]. Banding was poorly developed or entirely absent in most of the Neoproterozoic BIFs. Neoproterozoic BIFs are intimately associated with glaciomarine deposits and may be interbedded with manganese (Mn) deposits as well [63,65]. The atypical association between BIFs and Mn-rich sedimentation has been regarded by several previous authors as a strong indication of the GOE [134–136]. Another significant difference is that the iron-oxide of Neoproterozoic BIFs is only hematite [65]. Additionally, Neoproterozoic BIFs contain dropstones and faceted pebbles [63]. Neoproterozoic BIFs in different areas have different lithological assemblages, ore-bearing stratigraphy, and metamorphism degrees, but most of them have

the following common characteristics: (a) One or two groups of glaciated sedimentary formations are included in the sedimentary sequences and usually have moraines; (b) the large cap carbonate sequences overlays the above glacial sedimentary formations.

There is much debate about the reappearance of Neoproterozoic BIFs, which is acknowledged to be closely associated with glacial events. It is recognized that there are at least three Neoproterozoic glaciations, namely, Sturtian (~700 Ma), Marinoan (~600 Ma), and Gaskiers (~580 Ma) [34,136]. The extent of first two continental glaciations coincided with the abundance of BIFs [65], so some scholars presumably ascribed the formation of Neoproterozoic BIFs to the "Snowball Earth" hypothesis [65,137,138]. According to the "Snowball Earth" model, an extensive near-global ice cover sealed the oceans off from the atmosphere [34,65], causing anoxic and stagnant ocean. The glacial cover prevented the sulfate flux to the ancient ocean and possibly produced the anhydrite–magnetite redox buffer, resulting in higher Fe/S ratios in hydrothermal fluids, which promoted the accumulation and deposition of the magnitude of iron and precipitated to BIFs after the end of glacial events [79]. However, not all Neoproterozoic BIFs are glaciogenic [139], such as the formation of Shilu BIFs in Hainan, China at 850 Ma [140–142]; the BIFs in the Middle Tianshan Mountains in China ~760 Ma [143]; and the Arab-Nubian Shield BIFs at 750 Ma [144], all of which appeared before the glacial period. Therefore, the snowball Earth hypothesis cannot explain all the BIF mechanism. Some of the Neoproterozoic BIFs, which are consistent with the global glacial epoch (720~635 Ma), occurred during the interglacial period rather than the glacial period, and their formation process and mechanism are rather similar to the Blood Falls of modern Antarctic glaciers [145,146]. Alternatively, studies have shown that the formation of Neoproterozoic BIFs is strongly associated with the breakup of the Rodinia supercontinent [3,146,147]. In the Rodinian supercontinent restoration map, these Neoproterozoic BIFs were mainly distributed in the Rodinian supercontinent rifted basin or the basin margin [3]. Nevertheless, regardless of the intimate association between Neoproterozoic BIFs and glaciation, the formation of Neoproterozoic BIFs is attributed to submarine volcanism, rift exhalative sedimentation, sulfur reduction, and tectono-hydrothermal activities in silled basins [3,144,147,148].

4.4. Rare Phanerozoic BIFs

Previous studies suggested that atmospheric oxygen approached the modern atmosphere level at the beginning of the Phanerozoic [149], and the ocean began to oxidize. However, recent studies have inferred that it was after POE that the oxygen content reached the modern atmospheric level, and the ocean was generally oxidized [150–152].

Relevant scientific evidence shows that there were several oceanic anoxia events (OAE) during the Phanerozoic [99,132,153,154]. Although OAE resulted in sulfide oceans, researchers have found that anoxic and iron-rich (limited) oceans also occurred, as found in iron component studies (Sperling et al., 2015). Examples include the Late Permian Arabian [153], Cretaceous Morocco, and the central Pacific subtropical region [99]. Cambrian BIFs in Western Kunlun mountains in China [17]; Devonian BIFs [155] in western Siberia; Paleozoic La Endier iron ore [156]; Shikebutai iron deposit in Western Tianshan in China [157]; and the Quaternary BIFs [18] of Milos Island, Greece indicate the emergence of a limited, short-term, oxygen-poor, and iron-rich ocean in Phanerozoic. These Phanerozoic BIFs were volumetrically small and mainly formed in closed and semi-closed basins, such as island arcs and rifts, which were strongly related to submarine volcanism and might be Algoma-type BIFs [18]. The occurrences of Phanerozoic BIFs indicate that most of the Phanerozoic ocean was oxidized, but it was locally short-term anoxic and iron-rich, suggesting that the redox state and chemical composition of seawater changed dynamically in space and time during the Phanerozoic.

5. Discussions

As mentioned above, the formation of BIFs is closely related to major geological events, such as GOE, NOE, Snowball Earth, and continental crust accretion. GOE is one of the

most significant geological events in the history of the Earth. The rise of free oxygen in the Earth's atmosphere and oceans enabled the evolution of aerobic life. The biological, tectonic, and geochemical mechanisms that determined the stepwise pattern of GOE are still debated. A popular hypothesis is that oxygenic photosynthesis in microbial mats contribute a substantial source for the GOE. The latest research finds that increases in daylength could influenced the Earth's oxygenation, particularly around GOE [158]. GOE changed the composition of minerals on Earth and made possible the emergence of lives in the future [159]. From the perspective of the origin of life, biological processes and life on Earth in general are the most direct and probably the strongest link to the history of oxygen on Earth's surface, first through photosynthesis and second as a beneficiary of increasing oxygen levels in the case of respiring organisms. The development of the modern Earth System and the evolution of complex life were therefore direct consequences of the emergence of photosynthesizing cyanobacteria probably during the Archean–Proterozoic transition. After about 1.9 Ga, the first eukaryotes seem to have made their appearance, but remained highly conservative throughout much of the Proterozoic [159,160]. The time span that stretches from the late Neoproterozoic through to the mid-Cambrian (~800–501 Ma) witnessed increases in the diversity of acritarchs and other protistan morphotypes in fossil assemblages [160,161], heralding the evolution of architecturally complex bauplans and metazoans [162–172]. There are two major steps in the oxygenation of the Earth's surface that broadly correlate with the most important biological upgrades; first, from prokaryotes to eukaryotes around the GOE, and then from single-celled to complex, multicellular organisms in the Neoproterozoic. During the latter half of the Ediacaran period (635~542 Ma), the atmosphere and oceans were oxygenated to a higher degree than previously and there were dramatic changes in the biological world that culminated in the so-called "Cambrian explosion" with the appearance of large, complex life forms. Opinions as to the history of life origin, evolution, and diversification vary widely ([160] and references therein). Here, we highlighted a detailed study revealing a link between BIFs and major oxidation events on Earth (GOE and NOE) and deduced that the precipitation of BIFs was closely related to marine magmatic–hydrothermal activities.

5.1. GOE

Previous studies demonstrated that massive BIF deposits took place during the GOE. However, the latest detailed geochronology of BIFs shows that GOE (2.4–2.1 Ga) corresponds to the trough of BIFs (Figure 6a,c), and only a small number of BIFs formed during the GOE period, for example, BIFs in Yuanjiacun, North China Craton [173], and GIFs in Timeball Hill, South Africa [148]. However, the geochemical and mineralogical characteristics of BIFs changed significantly before and after the GOE, the fractionation of light and heavy REE in BIFs became more pronounced, and positive Ce anomalies appeared in some BIFs [20]. Moreover, the hematite in BIFs also increased significantly, and massive GIFs occurred [3]. Before 2.3 Ga, Fe ions in Fe-silicate were mainly Fe^{2+}, while after 2.3 Ga, Fe-silicate in BIFs exhibited mixed valence state. In addition, after GOE (about 1.88 Ga), BIFs pulsating peaks occurred (e.g., Animikie BIFs in North America, Frere BIFs in Western Australia) [35].

In the late Neoproterozoic, studies on C-S-Sr isotopes, iron components, and redox sensitive elements (such as U, Mo, and V) all showed that atmospheric oxygen had undergone a second significant rise (NOE) [32] (Figure 6a). The specific process, starting time, and controlling factors of the event have not been determined. The presence of Neoproterozoic BIFs (800 to 600 M years) is closely related to the "Snowball Earth" event [7,34,118], coupled with NOE (Figure 6a,c). Although GOE just corresponds to the trough of BIF deposition, about 60% of the global BIFs were formed before the GOE (2.5 Ga) [37] (Figure 6a,c). A commonly held view is that the formation of BIFs is related to GOE. However, after GOE (1.88 Ga), BIFs appeared discontinuously [35], suggesting that the relationship between the formation of BIFs and GOE still needs to be further researched. The Middle Proterozoic (1.8~0.8 Ga) is considered to be the Earth's middle age. It is assumed that during this

period, the oceans were completely oxidized [70] or the deep sea was vulcanized [104], resulting in a large depletion of BIFs. However, in recent years, it has been presumed that the deep ocean environment during the whole Mesoproterozoic was similar to the Archean counterpart, which still constituted an anoxic and iron-rich environment [131–133].

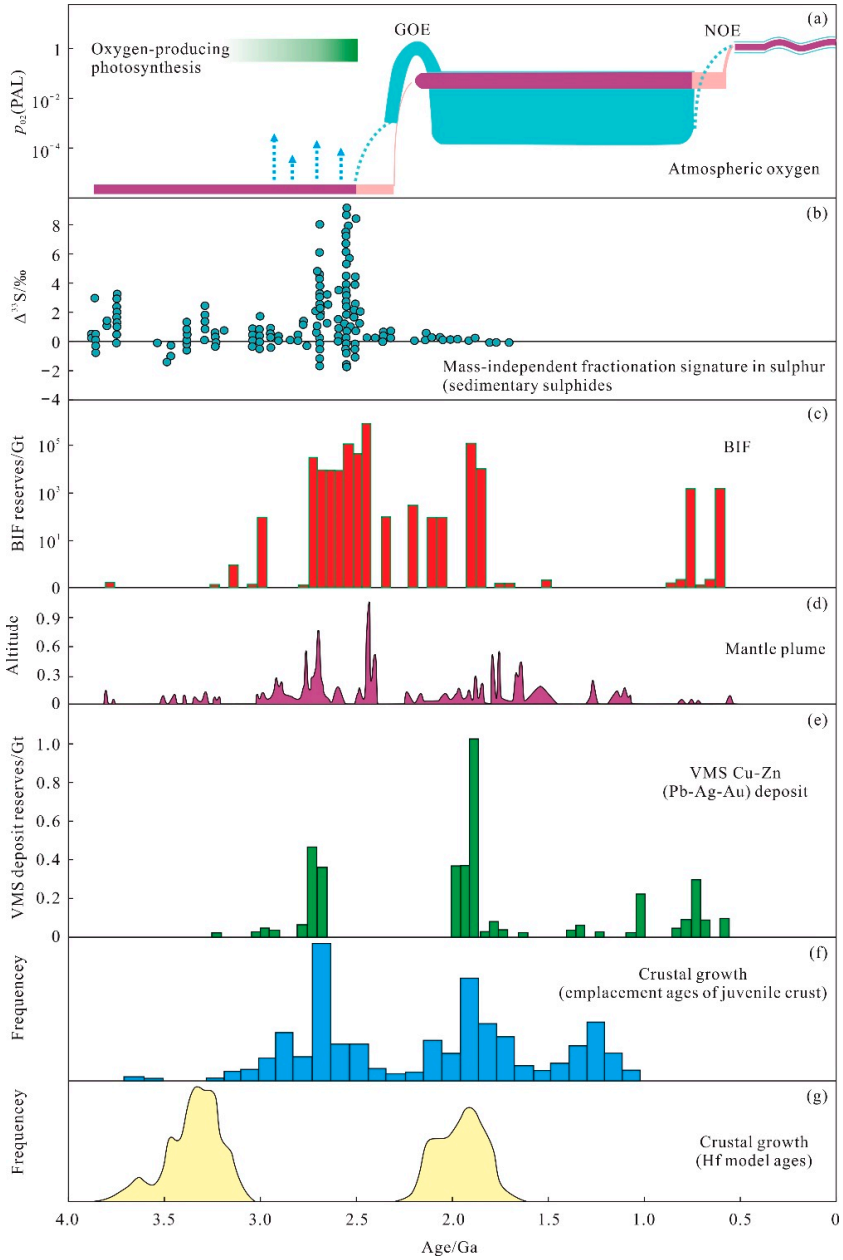

Figure 6. Summary of atmospheric oxygen concentration (**a**), Δ33S values of sulfides (**b**), the age distribution of BIF (**c**), VMS deposits (**d**), mantle plumes (**e**), and juvenile crust (**f**,**g**) for the Precambrian era. (**a**) Evolution of Earth's atmospheric oxygen concentration through time. The purple curve shows a classical, two-step view of atmospheric evolution, while the blue curve shows the emerging model (after [33]). (**b**) Plot of Precambrian Δ33S values of sulfides (after [35]). (**c**) Secular trend in the distribution of Precambrian BIF (after [3]). (**d**) Distribution of mantle plumes (after [3]), *y*-axis (height) is the sum of Gaussian time series for high-Mg intrusive rocks and layered intrusions, flood basalts, and dikes. (**e**) The distribution of VMS deposits over time (after [3]). (**f**) Distribution of U-Pb zircon ages for pre-1.0 Ga juvenile crust (after [35]). (**g**) Gaussian probability distribution of Hf model ages for zircons of pre-1.0 Ga (modified after [35]).

5.2. Submarine Magmatic–Hydrothermal Activities

Previous studies suggested that there is a strong correlation between BIFs and LIP. It can be seen from Figure 6e that the emplacement of multiple LIP at 1.88 Ga ago corresponds to a major episode in continental and oceanic crustal growth recorded by emplacement ages of juvenile igneous rocks [174,175]. There is strong evidence for widespread back arc magmatism and hydrothermal activity at 1.88 Ga ago, with a major peak in the formation of VMS deposits (Figure 6e) [3,176]. The presence of voluminous iron formations at 1.88 Ga ago is offered by their deposition during a period of intense igneous activity (Figure 6c–f). For example, between 1.89 and 1.87 Ga ago, extensive mafic and ultramafic magmatism occurred across the world, including the emplacement of dyke swarms and sills with the mineralization of Ni, Cu, and the platinum group elements, and, locally, basaltic flows, in the Superior, Wyoming, and Slave cratons in North America; the Dharwar and Bastar cratons in India; the Siberian craton; and the Kaapvaal and Zimbabwe cratons in southern Africa and in Baltica [177,178]. The emplacement of numerous LIP at that time might reflect the activity of multiple mantle plumes (a superplume event).

The ages of the volcanic and its associated BIFs units are often statistically the same [179–181]. The hydrothermal systems that generate VMS deposits also emit large volumes of dissolved iron into the deep ocean and trigger the deposition of BIFs [35–37]. Isley et al., (1999) [37] implicated that the mantle plume event occurred in four periods between 3.8 Ga and 1.6 Ga, which are 2.75~2.70 Ga, 2.50~2.40 Ga, 2.25~2.20 Ga, and 2.0~1.86 Ga, respectively. At least three of these periods enhanced the accumulation of BIFs. 2.5~2.40 Ga is the main period of the large-scale formation of BIFs as approximately 40% of the dated BIFs were deposited in this interval [3]. The other three periods also had different levels of BIFs (Figure 6d).

The symbiosis of Precambrian VMS and BIFs has been reported in many places around the world, such as the Abitibi greenstone belt in North America (Thurston et al., 2008) and the Isua greenstone belt in West Greenland [182,183]; Arizona and the Superior region [138]; the Carajas region of Brazil [184]; Neiqiu, Hebei, China [185]; Qingyuan, Liaoning, China [186,187]; and Wutai, Shanxi, China [187]. In these areas, BIFs are formed in VMS system margin facies [3] and the mass occurrences of BIFs are synchronous with that of the VMS spatially and temporally (Figure 6e). Units from the Barberton Mountain Land also contain massive sulfides or collapsed hydrothermal chimney deposits, indicating there was a proximal, high-temperature hydrothermal source for the iron [188]. Some Algoma-type BIFs, for example, the Boston iron formation and the Helen iron formation (Superior craton), have greater thicknesses (some of which exceed 1 km) but are also intercalated with volcanic flows and pyroclastics. These thicker BIFs also occur in associations with a range of volcanic compositions, from (ultra)mafic through felsic [184,185,189]. BIFs in Isua (Greenland) at 1.8 Ga is a symbiosis with VMS copper sulfide deposits in mafic/felsic metamorphic volcanic rocks and a metamorphic sedimentary rock series. Large-scale BIFs and a small number of copper sulfide deposits occurred within an area of more than 100 square kilometers [183]. The Abitibi of North America is the largest and most intact greenstone belt in the world, where the arc magma activity occurred during 2735~2670 Ma and lasted for 65 Ma. Dome structure, Komatites, and basalts are widely developed in Abitibi greenstone belt. The Noranda volcanogenic massive Cu-Pb-Zn sulfide deposit has a reserve of more than 100 million tons, which is the largest VMS deposits in the world. Thurston et al., (2008) [182] found that the VMS deposits in the ~2.7 Ga Abitibi greenstone belt were closely associated with BIFs, and from west to east, the VMS deposits gradually transitioned to BIFs deposits. In the Paleoproterozoic metamorphic volcano-sedimentary rock series in the Jerome area, Arizona, USA, BIF and VMS deposits are closely related as most of the BIFs occurred in the periphery of VMS deposits, showing a transitional spatial relationship. In some cases, the BIFs occur in the hanging wall of VMS deposits, such as the "iron hat" [138]. Numerous VMS deposits occurred in the Paleoproterozoic metamorphic volcanic zone in Superior craton. There are 24 large Cu-Zn VMS deposits in this area, of which the largest is the Flin Flon deposit with total metal resources of

62.4 Mt [190]. The chronology study shows that the main formation age of these VMS deposits is 1.92~1.88 Ga. Comparatively, the formation age of the BIFs in the most typical Superior craton is 1.89~1.84 Ga [35,191]. Moreover, the Hongtoushan VMS copper-Zn deposit occurred in the Neoarchaean Qingyuan greenstone belt in the northern margin of the North China Craton, where the contemporaneous BIFs are also developed [45].

Zhang et al., (2020) [45] proposed that the symbiotic mineralization of BIFs and VMS has the following characteristics: VMS polymetallic deposits and BIFs occur in the same volcanic-sedimentary systems and spatially restrict each other. VMS deposits usually occur in the bottom floor of BIFs sequences and occasionally in the upper part of BIFs sequences. It is further indicated that VMS and BIFs may share the same submarine hydrothermal system that provides ore-forming materials for both BIFs and VMS [7,45]. According to Rasmussen et al., (2012) [35], a large amount of BIF deposition in North America at 1.88 Ga was related to the global mafic-ultramafic magmatic activity, rapid continental crust proliferation, mantle depletion, and VMS deposition (Figure 6e–g).

The authors suggested that BIFs are closely associated with submarine magmatic–hydrothermal activities, especially Algoma-type BIFs, which usually occur in Precambrian volcanic sedimentary rock sequences [1,3]. Volcanic associations can be even present in the country rocks of Superior-type BIFs. Examples include the BIFs of the Hamersley Group in Western Australia and the BIFs of Kuruman in South Africa. Barley et al., (1997) [36] first noted the correlation between BIFs and mafic volcanism and proposed that the intrusion of large igneous provinces caused the precipitation of BIFs. Rasmussen et al., (2012) [35] pointed out that the sudden occurrence of large-scale BIF at ~1.88 Ga coincided with the intense submarine volcanism and hydrothermal activity. Rapitan BIFs in Canada was coincide with Franklin magma, both at 715 Ma [192]. Cox et al., (2013) [6] assumed that most Neoproterozoic BIFs were closely related to volcanism, which provided prerequisites for precipitation of BIFs. Chi Fu et al., (2018) [18] reported that the formation of BIFs in the early Quaternary on the Greek island of Milos was related to submarine volcanism. Similarly, modern polymetallic sediments are also associated with the seafloor volcanism [3,6]. Although iron from hydrothermal vents in modern oceans can precipitate directly at the marine-ocean crust interface, iron can also migrate hundreds of kilometers and precipitate [3]. On the other hand, strong submarine magmatic–hydrothermal activity not only provides large amounts of iron but also provides H_2, H_2S, SO_2, CO_2, and Mn to alter the redox state of the ocean and enhance the accumulation of BIFs [6,35]. Poulton et al., (2011) [132] showed that the addition of a large amount of submarine hydrothermal fluid in the deep sea would promote the development of the iron-rich ocean, thus benefitting the mass accumulation and precipitation of iron.

5.3. Perspectives

Since BIFs have undergone diagenesis and metamorphism [2], their primary nature and mineralogy can be deduced from ambiguous sedimentary structures, mineral paragenesis, and stratigraphy. Furthermore, as chemical sedimentary rocks, the sedimentary ages of BIFs are difficult to accurately determine, which hampers the in-depth understanding of the genesis of BIFs. BIFs have distinctive rhythmic bands, but the formation mechanism of bands is still obscure. The ages of the BIFs are coupled with major geological events, such as earth oxidation events, as well as large-scale submarine magmatic–hydrothermal activities, but how these geological events restricted the formation of BIFs needs to be further studied. Extensive studies suggest that BIFs may have a biological origin. However, due to the ancient age of BIFs, it is difficult to preserve microorganisms in the process of sedimentation, diagenesis, and later metamorphism evolution, resulting in mutilated biological information.

In the future research, we will focus on the following aspects:

- Element migration and enrichment in metamorphic and mineralization processes.
- The relationship between metamorphic, supercontinental events, and GOE.

- What are the fluid sources of mineralization under different metamorphism degrees, especially in the middle and high degree?
- The influence of ore-forming fluid migration, oxygen fugacity, and variable CO_2 on BIFs and enrichment.
- The mechanism of environmental mutation and metamorphism on the accumulation of ore-forming elements and BIF mineralization. There is still much space for exploration and study.

The development of geological big data, precise geochronology, simulation experiments, new techniques of non-traditional stable isotopes (Fe, Cr, Mo, and Cu, etc.), and an in-depth understanding of the ocean hydrothermal system will provide new insight that will allow one to address the hot and difficult problem regarding the genesis of BIF and its complex relationship with the lithosphere, atmosphere, hydrosphere, and biosphere.

6. Conclusions

BIFs are distinctive Precambrian chemical sedimentary rocks with mineral layers of variable thickness, including magnetite, hematite, chert, siderite, ankerite, and other related minerals formed mostly in Precambrian eras. The Precambrian BIFs can be divided into the Algoma type, which is closely related to volcanism, and the Superior type, which is far from the eruptive centers. Neoproterozoic BIFs are mainly of the Rapitan type, which is closely related to the "Snowball Earth" event, and a minor amount of them might be of the Algoma type. The core of BIFs is the oxidation of Fe^{2+} to Fe^{3+} in seawater, including biological oxidation and abiotic oxidation. Mega BIF deposition occurred on the eve of GOE, and Neoproterozoic BIFs appeared to be highly coupled with NOE. The formation of BIFs is closely related to magmatic–hydrothermal activities on the seafloor. In addition, microorganisms also play a crucial role, directly or indirectly controlling the formation and their preservation of BIFs in diagenetic processes. The absence of BIFs in the Mesoproterozoic (1.8~0.8 Ga) and Phanerozoic is mainly related to the changes of the redox state and the chemical composition of the ocean. The preponderance of Precambrian and Neoproterozoic BIFs, and the deficiency of BIFs in the Mesoproterozoic and Phanerozoic, are strongly associated with major geological events. These major geological events interact with each other, jointly constraining the evolution of the atmosphere, marine environment, and biological and geodynamical process.

Author Contributions: Conceptualization, J.Y. and K.X.; methodology, J.Y., K.X. and H.L.; validation, H.L. and K.X.; formal analysis J.Y., K.X. and H.L.; investigation, J.Y., K.X. and H.L.; resources, J.Y.; data curation: J.Y.; writing—original draft preparation, J.Y; writing—review and editing, H.L.; visualization, J.Y.; and supervision, K.X. All authors have read and agreed to the published version of the manuscript.

Funding: This work is financially supported by the Geological Survey Project of CGS (China Geological Survey) (No. DD20230055) and the National Key Research and Development Program of China (Nos. 2017YFC0601501 and 2018YFC0603904).

Data Availability Statement: All relevant data are within the paper.

Acknowledgments: We would like to acknowledge XiaoJuan Wang for the figure drawing. Furthermore, we would like to thank the reviewers for their thorough work, which significantly improved the quality of our paper.

Conflicts of Interest: The authors declare no conflict of interest.

References

1. Gross, G.A. A classification of iron formations based on depositional environments. *Can. Mineral* **1980**, *18*, 215–222.
2. James, H.L. Sedimentary facies of iron-formation. *Econ. Geol.* **1954**, *49*, 235–249. [CrossRef]
3. Bekker, A.; Slack, J.F.; Planavsky, A.; Krapež, B.; Hofmann, A.; Konhauser, K.O.; Rouxel, O.J. Iron formation: The sedimentary product of a complex interplay among mantle, tectonic, oceanic, and biospheric processes. *Econ. Geol.* **2010**, *105*, 467–508. [CrossRef]

4. O'Neil, J.; Carlson, R.W.; Francis, D.; Stevens, R.K. Neodymium-142 evidence for Hadean mafic crust. *Science* **2008**, *321*, 1828–1831. [CrossRef] [PubMed]
5. Ilyin, A.V. Neoproterozoic banded iron formations. *Lithol. Miner. Resour.* **2009**, *44*, 78–86. [CrossRef]
6. Cox, G.M.; Halverson, G.P.; Minarik, W.G.; LeHeron, D.P.; Macdonald, F.A.; Bellefroid, E.J.; Strauss, J.V. Neoproterozoic iron formation: An evaluation of its temporal, environmental and tectonic significance. *Chem. Geol.* **2013**, *362*, 232–249. [CrossRef]
7. Klein, C. Some Precambrian banded iron-formations (BIFs) from around the world: Their age, geologic setting, mineralogy, metamorphism, geochemistry, and origin. *Am. Mineral* **2005**, *90*, 1473–1499. [CrossRef]
8. Heard, A.W.; Dauphas, N.; Hinz, I.L.; Johnson, J.E.; Blanchard, M.; Alp, E.E.; Hu, M.Y.; Zhao, J.; Lavina, B.; Fornace, M.E.; et al. Isotopic Constraints on the Nature of Primary Precipitates in Archean–Early Paleoproterozoic Iron Formations from Determinations of the Iron Phonon Density of States of Greenalite and 2L- and 6L-Ferrihydrite. *ACS Earth Space Chem.* **2023**, 1–16. [CrossRef]
9. Li, H.M.; Zhang, Z.J.; Li, L.L.; Zhang, Z.C.; Chen, J.; Yao, T. Types and general characteristics of the BIF-related iron deposits in China. *Ore Geol. Rev.* **2014**, *57*, 264–287. [CrossRef]
10. Zhang, Z.C.; Hou, T.; Santosh, M.; Li, H.M.; Li, J.; Zhang, Z.; Song, X.; Wang, M. Spatial-temporal distribution and tectonic settings of the major iron deposits in China: An overview. *Ore Geol. Rev.* **2014**, *57*, 247–263. [CrossRef]
11. Richards, S.M. The banded iron formations at Broken Hill, Australia, and their relationship to the lead-zinc orebodies. *Econ. Geol.* **1966**, *61*, 72–96. [CrossRef]
12. Slack, J.F.; Grenne, T.; Bekker, A. Seafloor-hydrothermal Si-Fe Mn exhalites in the Pecos greenstone belt, New Mexico, and the redox state of ca. 1720 Ma deep seawater. *Geosphere* **2009**, *5*, 302–314. [CrossRef]
13. Comin-Chiaramonti, P.; Girardi, V.A.V.; De Min, A.; Boggiani, P.C.; Correia, C.T. Iron-rich formations at the Cerro Manomó region, southeastern Bolivia: Remnant of a BIF? *Episodes* **2011**, *34*, 177–185. [CrossRef]
14. Lascelles, D.F. Plate tectonics caused the demise of banded iron formations. *Appl. Earth Sci. Imm Trans.* **2013**, *122*, 230–241. [CrossRef]
15. Yang, X.Q.; Zhang, Z.H.; Duan, S.G.; Zhao, X.M. Petrological and geochemical features of the Jingtieshan banded iron formation (BIF): A unique type of BIF from the Northern Qilian Orogenic Belt, NW China. *J. Asian Earth Sci.* **2015**, *113*, 1218–1234. [CrossRef]
16. Yang, X.Q.; Zhang, Z.H.; Guo, S.F.; Chen, J.; Wang, D.C. Geochronological and geochemical studies of the metasedimentary rocks and diabase from the Jingtieshan deposit, north Qilian, NW China: Constraints on the associated banded iron formations. *Ore Geol. Revs* **2016**, *73*, 42–58. [CrossRef]
17. Li, Z.Q.; Zhang, L.C.; Xue, C.J.; Zhu, M.T.; Robbins, L.J.; Slack, J.F.; Planavsky, N.J.; Konhauser, K.O. Earth's youngest banded iron formation implies ferruginous conditions in the early Cambrian ocean. *Sci. Rep.* **2018**, *8*, 9970. [CrossRef]
18. Chi Fru, E.; Kilias, S.; Ivarsson, M.; Rattray, J.E.; Gkika, K.; McDonald, I.; He, Q.; Broman, C. Sedimentary mechanisms of a modern banded iron formation on Milos Island, Greece. *Solid Earth* **2018**, *9*, 573–598. [CrossRef]
19. Cloud, P.E. Paleoecological significance of the banded iron formation. *Econ. Geol.* **1973**, *68*, 1135–1143. [CrossRef]
20. Planavsky, N.; Bekker, A.; Rouxel, O.J.; Kamber, B.; Hofmann, A.; Knudsen, A.; Lyons, T.W. Rare Earth Element and yttrium compositions of Archean and Paleoproterozoic Fe formations revisited: New perspectives on the significance and mechanisms of deposition. *Geochim. Cosmochim. Acta* **2010**, *74*, 6387–6405. [CrossRef]
21. Johnson, J.E.; Molnar, P.H. Widespread and persistent deposition of iron formations for two billion years. *Geophys. Res. Lett.* **2019**, *46*, 3327–3339. [CrossRef]
22. Posth, N.R.; Canfield, D.E.; Kappler, A. Biogenic Fe(III) minerals: From formation to diagenesis and preservation in the rock record. *Earth-Sci. Rev.* **2014**, *135*, 103–121. [CrossRef]
23. Konhauser, K.O.; Planavsky, N.J.; Hardisty, D.S.; Robbins, L.J.; Warchola, T.J.; Haugaard, R.; Lalonde, S.; Partin, C.A.; Oonk, P.B.H.; Tsikos, H.; et al. Iron formations: A global record of Neoarchaean to Palaeoproterozoic environmental history. *Earth-Sci. Rev.* **2017**, *172*, 140–177. [CrossRef]
24. Yang, X.Q.; Zhang, Z.H.; Santosh, M.; Duan, S.G.; Liang, T. Anoxic to suboxic Mesoproterozoic ocean: Evidence from iron isotope and geochemistry of siderite in the Banded Iron Formations from North Qilian, NW China. *Precambrian Res.* **2018**, *307*, 115–124. [CrossRef]
25. Johnson, C.M.; Beard, B.L.; Klein, C.; Beukes, N.J.; Roden, E.E. Iron isotopes constrain biologic and abiologic processes in banded iron formation genesis. *Geochim. Cosmochim. Acta* **2008**, *72*, 151–169. [CrossRef]
26. Heimann, A.; Johnson, C.M.; Beard, B.L.; Valley, J.W.; Roden, E.E.; Spicuzza, M.J.; Beukes, N.J. Fe, C, and O isotope compositions of banded iron formation carbonates demonstrate a major role for dissimilatory iron reduction in ~2.5 Ga marine environments. *Earth Planet Sci. Lett.* **2010**, *294*, 8–18. [CrossRef]
27. Zhai, M.G. Multi-stage crustal growth and cratonization of the North China Craton. *Geosci. Front.* **2014**, *5*, 457–469. [CrossRef]
28. Zhang, L.C.; Zhai, M.G.; Wan, Y.S.; Guo, J.H.; Dai, Y.P.; Wang, C.L.; Liu, L. Study of the Precambrian BIF-iron deposits in the North China Craton: Progresses and questions. *Acta Petrol. Sin.* **2012**, *28*, 3431–3445. (In Chinese with English abstract)
29. Beukes, N.J. Dating the rise of atmospheric oxygen. *Nature* **2004**, *427*, 117–120.
30. Bekker, A.; Kaufman, A.J. Oxidative forcing of global climate change: A biogeochemical record across the oldest Paleoproterozoic ice age in North America. *Earth Planet. Sci. Lett.* **2007**, *258*, 486–499. [CrossRef]
31. Holland, H.D. Volcanic gases, black smokers, and the Great Oxidation Event. *Geochim. Cosmochim. Acta* **2002**, *66*, 3811–3826. [CrossRef]

32. Och, L.M.; Shields-Zhou, G.A. The Neoproterozoic oxygenation event: Environmental perturbations and biogeochemical cycling. *Earth-Sci. Rev.* **2012**, *110*, 26–57. [CrossRef]
33. Lyons, T.W.; Reinhard, C.T.; Planavsky, N.J. The rise of oxygen in earth's early ocean and atmosphere. *Nature* **2014**, *506*, 307–315. [CrossRef]
34. Hoffman, P.F.; Kaufman, A.J.; Halverson, G.P.; Schrag, D.P. A Neoproterozoic snowball earth. *Science* **1998**, *281*, 1342–1346. [CrossRef]
35. Rasmussen, B.; Fletcher, I.R.; Bekker, A.; Muhling, J.R.; Gregory, C.J.; Thorne, A.M. Deposition of 1.88-billion-year-old iron formations as a consequence of rapid crustal growth. *Nature* **2012**, *484*, 498–501. [CrossRef]
36. Barley, M.E.; Pickard, A.L.; Sylvester, P.J. Emplacement of a large igneous province as a possible cause of banded iron formation 2.45 billion years ago. *Nature* **1997**, *385*, 55–58. [CrossRef]
37. Isley, A.E.; Abbott, D.H. Plume-related mafic volcanism and the deposition of banded iron formation. *J. Geophys. Res. Solid Earth* **1999**, *104*, 15461–15477. [CrossRef]
38. Glikson, A.; Vickers, J. Asteroid mega-impacts and Precambrian banded iron formations: 2.63 Ga and 2.56 Ga impact ejecta/fallout at the base of BIF/argillite units, hamersley basin, pilbara craton, western Australia. *Earth Planet. Sci. Lett.* **2007**, *254*, 214–226. [CrossRef]
39. Huston, D.L.; Logan, G.A. Barite, BIFs and bugs: Evidence for the evolution of the Earth's early hydrosphere. *Earth Planet. Sci. Lett.* **2004**, *220*, 41–55. [CrossRef]
40. Clout, J.M.F. Iron formation-hosted iron ores in the Hamersley Province of western Australia. *Appl. Earth Sci.* **2006**, *115*, 115–125. [CrossRef]
41. Li, B.L.; Huo, L.; Li, Y.S. Several problems involved in the study of banded iron formations (BIFs). *Acta Mineral. Sin.* **2007**, *27*, 205–210. (In Chinese with English abstract)
42. Li, Y.H.; Hou, K.J.; Wan, D.F.; Zhang, Z.J.; Le, G.L. Formation mechanism of Precambrian banded iron formation and atmosphere and ocean during early stage of the Earth. *Acta Geol. Sin.* **2010**, *84*, 1359–1373. (In Chinese with English abstract)
43. Li, Y.H.; Hou, K.J.; Wan, D.F.; Zhang, Z.J. A compare geochemistry study for Algoma—And Superior-type banded iron formations. *Acta Petrol. Sin.* **2012**, *28*, 3513–3519. (In Chinese with English abstract)
44. Zhang, L.C.; Peng, Z.D.; Zhai, M.G.; Tong, X.X.; Zhu, M.T.; Wang, C.L. Tectonic setting and genetic relationship between BIF and VMS- in the Qingyuan Neoarchean Greenstone Belt, northern North China Craton. *Earth Sci.* **2020**, *45*, 1–16. (In Chinese with English abstract)
45. Wang, C.L.; Zhang, L.C.; Liu, L.; Dai, Y.P. Research progress and some problems deserving further discussion of Precambrian iron formations. *Miner. Depos.* **2012**, *31*, 1311–1325. (In Chinese with English abstract)
46. Yang, X.Q.; Li, H.M.; Li, L.X.; Yao, T.; Chen, J.; Liu, M.J. Geochemical characteristics of banded iron formations in Liaoning Eastern Hebei area: I. Characteristics of major elements. *Acta Petrol. Sin.* **2014**, *30*, 1218–1238. (In Chinese with English abstract)
47. Liu, L.; Zhang, L.C.; Dai, Y.P. Research progress on the genesis of BIF. *Chin. J. Geol.* **2014**, *29*, 1018–1033. (In Chinese with English abstract)
48. Bjerrum, C.J.; Canfield, D.E. Ocean productivity before about 1.9 Gyr ago limited by phosphorus adsorption onto iron oxides. *Nature* **2002**, *417*, 159–162. [CrossRef]
49. Tong, X.X.; Wang, C.L.; Peng, Z.D.; Nan, J.B.; Huang, H.; Zhang, L.C. Primary mineral information and depositional models of relevant mineral facies of the Early Precambrian BIF-A preliminary review. *Adv. Earth Sci.* **2018**, *33*, 152–165. (In Chinese with English abstract)
50. Hall, W.D.M.; Goode, A.D.T. The early Proterozoic Nabberu basin and associated iron formations of Western Australia. *Pre Cambr. Res.* **1978**, *7*, 129–184. [CrossRef]
51. Beukes, N.J. Sedimentology of the Kuruman and Griquatown iron-formations, Transvaal Supergroup, Griqualand West, South Africa. *Precambrian Res.* **1984**, *24*, 47–84. [CrossRef]
52. Derry, L.A.; Jacobsen, S.B. The chemical evolution of Precambrian seawater-evidence from REEs in banded iron formations. *Geochim. Cosmochim. Acta* **1990**, *54*, 2965–2977. [CrossRef]
53. Danielson, A.; Möller, P.; Dulski, P. The europium anomalies in banded iron formations and the thermal history of the oceanic crust. *Chem. Geol.* **1992**, *97*, 89–100. [CrossRef]
54. Barrett, T.J.; Fralick, P.W.; Jarvis, I. Rare-earth-element geochemistry of some Archean iron formations north of Lake Superior, Ontario. *Can. J. Earth Sci.* **1988**, *25*, 570–580. [CrossRef]
55. Hagemann, S.G.; Angerer, T.; Duuring, P. BIF-hosted iron mineral system: A review. *Ore Geol. Rev.* **2016**, *76*, 317–359. [CrossRef]
56. Gross, G.A. Tectonic systems and the deposition of iron-formation. *Precambrian Res.* **1983**, *20*, 171–187. [CrossRef]
57. Weill, D.F.; Drake, M.J. Europium anomaly in plagioclase feldspar: Experimental results and semiquantitative model. *Science* **1973**, *180*, 1059–1060. [CrossRef]
58. Ching-Oh, S.; Williams, R.J.; Shine-Soon, S. Distribution coefficients of Eu and Sr for plagioclase-liquid and clinopyroxene-liquid equilibria in oceanic ridge basalt: An experimental study. *Geochim. Cosmochim Acta* **1974**, *38*, 1415–1433. [CrossRef]
59. Drake, M.J.; Weill, D.F. Partition of Sr, Ba, Ca, Y, Eu^{2+}, Eu^{3+}, and other REE between plagioclase feldspar and magmatic liquid: An experimental study. *Geochim. Cosmochim. Acta* **1975**, *39*, 689–712. [CrossRef]
60. Klein, C.; Ladeira, E.A. Geochemistry and mineralogy of Neoproterozoic banded iron-formations and some selected siliceous manganese formations from the Urucum District, Matto Grosso do Sul, Brazil. *Econ. Geol.* **2004**, *99*, 1233–1244. [CrossRef]

61. Force, E.R.; Eidel, J.J.; Maynard, J.B. *Sedimentary and Diagenetic Mineral Deposits: A Basin Analysis Approach to Exploration*; Reviews in Economic Geology; Society of Economic Geologists: Chelsea, MI, USA, 1991; Volume 5, 216p.
62. Klein, C.; Beukes, N.J. Sedimentology and geochemistry of the glaciogenic Late Proterozoic Rapitan Iron-formation in Canada. *Econ. Geol.* **1993**, *88*, 542–565. [CrossRef]
63. Viehmann, S.; Bau, M.; Bühn, B.; Dantas, E.L.; Andrade, F.R.D.; Walde, D.H.G. Geochemical characterisation of Neoproterozoic marine habitats: Evidence from trace elements and Nd isotopes in the Urucum iron and manganese formations, Brazil. *Precambrian Res.* **2016**, *282*, 74–96. [CrossRef]
64. Cloud, P.E. Significance of the Gunflint (Precambrian) microflora. *Science* **1965**, *148*, 27–35. [CrossRef] [PubMed]
65. Cloud, P.E. Atmospheric and hydrospheric evolution on the primitive Earth. *Science* **1968**, *160*, 729–736. [CrossRef] [PubMed]
66. Holland, H. *The Chemical Evolution of the Atmosphere and Oceans*; Princeton University Press: New York, NY, USA, 1984; p. 582.
67. Habicht, K.S.; Gade, M.; Thamdrup, B.; Berg, P.; Canfield, D.E. Calibration of sulfate levels in the Archean ocean. *Science* **2002**, *298*, 2372–2374. [CrossRef]
68. Johnson, C.M.; Beard, B.L.; Beukes, N.J.; Klein, C.; O'Leary, J.M. Ancient geochemical cycling in the Earth as inferred from Fe isotope studies of banded iron formations from the Transvaal Craton. *Contrib. Mineral. Petrol.* **2003**, *144*, 523–547. [CrossRef]
69. Planavsky, N.J.; Rouxel, O.J.; Bekker, A.; Hoffmann, A.; Little, C.T.; Lyons, T.W. Iron isotope composition of some Archean and Proterozoic iron formations. *Geochim. Cosmochim. Acta* **2012**, *80*, 158–169. [CrossRef]
70. Raiswell, R.; Canfield, D.E. The iron biogeochemical cycle past and present. *Geochem. Perspect.* **2012**, *1*, 1–2. [CrossRef]
71. Fryer, B.J.; Fyfe, W.S.; Kerrich, R. Archean volcanogenic oceans. *Chem. Geol.* **1979**, *24*, 25–33. [CrossRef]
72. Raye, U.; Pufahl, P.K.; Kyser, T.K.; Ricard, E.; Hiatt, E.E. The role of sedimentology, oceanography, and alteration on the δ56 Fe value of the Sokoman Iron Formation, Labrador Trough, Canada. *Geochim. Cosmochim. Acta* **2015**, *164*, 205–220. [CrossRef]
73. Zhou, S.T. *Geology of BIF-Related Iron Deposits in Anshan-Benxi District*; Geological Publishing House: Beijing, China, 1994; pp. 1–278. (In Chinese)
74. Li, W.; Beard, L.; Johnson, C.M. Biologically recycled continental iron is a major component in banded iron formations. *Proc. Natl. Acad. Sci. USA* **2015**, *112*, 8193–8198. [CrossRef]
75. Kang, N.; Schmidt, M.W. The melting of subducted banded iron formations. *Earth Planet. Sci. Lett.* **2017**, *476*, 165–178. [CrossRef]
76. Saito, M.A.; Noble, A.E.; Tagliabue, A.; Goepfert, T.J.; Lamborg, C.H.; Jenkins, W.J. Slow-preading submarine ridges in the South Atlantic as a significant oceanic iron source. *Nat. Geosci.* **2013**, *6*, 775–779. [CrossRef]
77. Viehmann, S.; Hoffmann, J.E.; Münker, C.; Bau, M. Decoupled Hf-Nd isotopes in Neoarchean seawater reveal weathering of emerged continents. *Geology* **2014**, *42*, 115–118. [CrossRef]
78. Cox, G.M.; Halverson, G.P.; Poirier, A.; Heron, D.L.; Strauss, J.V.; Stevenson, R. A model for Cryogenian iron formation. *Earth Planet. Sci. Lett.* **2016**, *433*, 280–292. [CrossRef]
79. Alexander, B.W.; Bau, M.; Andersson, P. Neodymium isotopes in Archean seawater and implications for the marine Nd cycle in Earth's early oceans. *Earth Planet. Sci. Lett.* **2009**, *283*, 144–155. [CrossRef]
80. Hannington, M.D.; Cornell, D.J.R.; Petersen, S. Sea-floor tectonics and submarine hydrothermal systems. *Econ. Geol.* **2005**, *100*, 111–141.
81. Kump, L.R.; Seyfried, W.E. Hydrothermal Fe fluxes during the Precambrian: Effect of low oceanic sulfate concentrations and low hydrostatic pressure on the composition of black smokers. *Earth Planet. Sci. Lett.* **2005**, *235*, 654–662. [CrossRef]
82. Isley, A. Hydrothermal plumes and the delivery of iron to banded iron formation. *J. Geol.* **1995**, *103*, 169–185. [CrossRef]
83. Wang, Y.; Xu, H.; Merino, E.; Konishi, H. Generation of banded iron formations by internal dynamics and leaching of oceanic crust. *Nat. Geosci.* **2009**, *2*, 781–784. [CrossRef]
84. Poulton, S.W.; Raiswell, R. The low-temperature geochemical cycle of iron: From continental fluxes to marine sediment deposition. *Am. J. Sci.* **2002**, *302*, 774–805. [CrossRef]
85. Lyons, T.W.; Severmann, S. A critical look at iron paleoredox proxies: New insights from modern euxinic marine basins. *Geochim. Cosmochim. Acta* **2006**, *70*, 5698–5722. [CrossRef]
86. Jacobsen, S.B.; Pimentel-Klose, M.R. Nd isotopic variations in Precambrian banded iron formations. *Geophys. Res. Lett.* **1988**, *15*, 393–396. [CrossRef]
87. Frei, R.; Bridgwater, D.; Rosing, M.; Stecher, O. Controversial Pb-Pb and Sm-Nd isotope results in the early Archean Isua (West Greenland) oxide iron formation: Preservation of primary signatures versus secondary disturbances. *Geochim. Cosmochim. Acta* **1999**, *63*, 473–488. [CrossRef]
88. Døssing, L.N.; Frei, R.; Stendal, H.; Mapeo, R.B.M. Characterization of enriched lithospheric mantle components in ∼2.7Ga banded iron formations: An example from the Tati greenstone belt, northeastern Botswana. *Precambrian Res.* **2009**, *172*, 334–356. [CrossRef]
89. Haugaard, R.; Frei, R.; Stendal, H.; Konhauser, K. Petrology and geochemistry of the ∼2.9 Ga Itilliarsuk banded iron formation and associated supracrustal rocks, West Greenland: Source characteristics and depositional environment. *Precambrian Res.* **2013**, *229*, 150–176. [CrossRef]
90. Wang, C.; Zhang, L.; Dai, Y.; Li, W. Source characteristics of the 2.5 Ga Wangjiazhuang banded iron formation from the Wutai greenstone belt in the North China Craton: Evidence from neodymium isotopes. *J. Asian Earth Sci.* **2014**, *93*, 288–300. [CrossRef]

91. Wang, C.; Wu, H.; Li, W.; Peng, Z.; Zhang, L.; Zhai, M. Changes of Ge/Si, REE+Y and Sm-Nd isotopes in alternating Fe- and Si-rich mesobands reveal source heterogeneity of the ~2.54 Ga Sijiaying banded iron formation in eastern Hebei, China. *Ore Geol. Rev.* **2017**, *80*, 363–376. [CrossRef]
92. Smith, A.J.B.; Beukes, N.J.; Gutzmer, J. The composition and depositional environments of Mesoarchean iron formations of the West Rand Group of the Witwatersrand Supergroup, South Africa. *Econ. Geol.* **2013**, *108*, 111–134. [CrossRef]
93. Hamade, T.; Konhauser, K.O.; Raiswell, R.; Goldsmith, S.; Morris, R.C. Using Ge/Si ratios to decouple iron and silica fluxes in Precambrian banded iron formations. *Geology* **2003**, *31*, 35–38. [CrossRef]
94. Frei, R.; Polat, A. Source heterogeneity for the major components of ∼3.7 Ga Banded Iron Formations (Isua Greenstone Belt, Western Greenland): Tracing the nature of interacting water masses in BIF formation. *Earth Planet. Sci. Lett.* **2007**, *253*, 266–281. [CrossRef]
95. Pokrovsky, O.S.; Pokrovski, G.S.; Schott, J.; Galy, A. Experimental study of germanium adsorption on goethite and germanium coprecipitation with iron hydroxide: X-ray absorption fine structure and macroscopic characterization. *Geochim. Cosmochim. Acta* **2006**, *70*, 3325–3341. [CrossRef]
96. Rouxel, O.; Galy, A.; Elderfield, H. Germanium isotopic variations in igneous rocks and marine sediments. *Geochim. Cosmochim. Acta* **2006**, *70*, 3387–3400. [CrossRef]
97. Poulton, S.W.; Henkel, S.; März, M.; Urquhart, H.; Flögel, S.; Kasten, S.; Damsté, J.S.S.; Wagner, T. A continental-weathering control on orbitally driven redox-nutrient cycling during Cretaceous Oceanic Anoxic Event 2. *Geology* **2015**, *43*, 963–966. [CrossRef]
98. Hou, K.; Ma, X.; Li, Y.; Liu, F.; Han, D. Chronology, geochemical, Si and Fe isotopic constraints on the origin of Huoqiu banded iron formation (BIF), southeastern margin of the North China Craton. *Precambrian Res.* **2017**, *298*, 351–364. [CrossRef]
99. Conway, T.M.; John, S.G.; Lacan, F. Intercomparison of dissolved iron isotope profiles from reoccupation of three GEOTRACES stations in the Atlantic Ocean. *Mar. Chem.* **2016**, *183*, 50–61. [CrossRef]
100. Thibon, T.; Blichert-Toft, J.; Tsikos, H.; Foden, J.; Albalat, E.; Albarede, F. Dynamics of oceanic iron prior to the Great Oxygenation Event. *Earth Planet. Sci. Lett.* **2019**, *506*, 360–370. [CrossRef]
101. Sumner, D.Y. Carbonate precipitation and oxygen stratification in late Archean seawater as deduced from facies and stratigraphy of the Gamohaan and Frisco formations, Transvaal Supergroup, South Africa. *Am. J. Sci.* **1997**, *297*, 455–487. [CrossRef]
102. Canfield, D.E. A new model for Proterozoic ocean chemistry. *Nature* **1998**, *396*, 450–453. [CrossRef]
103. Hoashi, M.; Bevacqua, D.C.; Otake, T.; Watanabe, Y.; Hickman, A.H.; Utsunomiya, S.; Ohmoto, H. Primary hematite formation in an oxygenated sea 3.46 billion years ago. *Nat. Geosci.* **2009**, *2*, 301–306. [CrossRef]
104. Frei, R.; Gaucher, C.; Poulton, S.W.; Canfield, D.E. Fluctuations in Precambrian atmospheric oxygenation recorded by chromium isotopes. *Nature* **2009**, *461*, 250–253. [CrossRef]
105. Cardona, T. Thinking twice about the evolution of photosynthesis. *Open Biol.* **2019**, *9*, 180246. [CrossRef]
106. Kendall, B.; Reinhard, C.D.; Lyons, T.D.; Kaufman, A.J.; Poulton, S.W.; Anbar, A.D. Pervasive oxygenation along late Archaean ocean margins. *Nat. Geosci.* **2010**, *3*, 646–652. [CrossRef]
107. Halevy, I.; Alesker, M.; Schuster, E.M.; Popovitz-Biro, R.; Feldman, Y. A key role for green rust in the Precambrian oceans and the genesis of iron formations. *Nat. Geosci.* **2017**, *10*, 135–139. [CrossRef]
108. Tsikos, H.; Siahi, M.; Rafuza, S.; Mhlanga, X.R.; Oonk, P.B.H.; Papadopoulos, V.; Boyce, A.J.P.; Mason, R.D.; Harris, C.D.; Gröcke, R.; et al. Carbon isotope stratigraphy of Precambrian iron formations and possible significance for the early biological pump. *Gondwana Res.* **2022**, *109*, 416. [CrossRef]
109. Ehrenreich, A.; Widdel, F. Anaerobic oxidation of ferrous iron by purple bacteria, a new type of phototrophic metabolism. *Appl. Environ. Microbiol.* **1994**, *60*, 4517–4526. [CrossRef]
110. Konhauser, K.O.; Hamade, T.; Raiswell, R.; Morris, R.C.; Ferris, F.G.; Southam, G.; Canfield, D.E. Could bacteria have formed the Precambrian banded iron formations? *Geology* **2002**, *30*, 1079–1082. [CrossRef]
111. Kappler, A.; Pasquero, C.; Konhauser, K.O.; Newman, D.K. Deposition of banded iron formations by anoxygenic phototrophic Fe (II) -oxidizing bacteria. *Geology* **2005**, *33*, 865–868. [CrossRef]
112. Canfield, D.E.; Zhang, S.; Wang, H.; Wang, X.; Zhao, W.; Su, J.; Bjerrum, C.J.; Haxen, E.R.; Hammarlund, E.A. Mesoproterozoic iron formation. *Proc. Natl. Acad. Sci.* **2018**, *115*, 3895–3904. [CrossRef]
113. Cairns-Smith, A.G. Precambrian solution photochemistry, inverse segregation, and banded iron formations. *Nature* **1978**, *276*, 807–808. [CrossRef]
114. Busigny, V.; Planavsky, N.J.; Goldbaum, E.; Lechte, M.A.; Feng, L.J.; Lyons, T.M. Origin of the Neoproterozoic Fulu iron formation, South China: Insights from iron isotopes and rare earth element patterns. *Geochim. Cosmochim. Acta* **2018**, *242*, 123–142. [CrossRef]
115. Lechte, M.A.; Wallace, M.W.; Ashleigh, V.S.H.; Planavsky, N. Cryogenian iron formations in the glaciogenic Kingston Peak Formation, California. *Precambrian Res.* **2018**, *310*, 443–462. [CrossRef]
116. Farquhar, J.; Savarino, J.; Airieau, S.; Thiemens, M.H. Observation of wavelength- sensitive mass- independent sulfur iso tope effects during SO_2 photolysis: Implications for the Early atmosphere. *J. Geophys. Res. Planets* **2001**, *106*, 32829–32839. [CrossRef]
117. Pavlov, A.A.; Kasting, J.F. Mass-independent fractionation of sulfur isotopes in Archean sediments: Strong evidence for an anoxic Archean atmosphere. *Astrobiology* **2002**, *2*, 27–41. [CrossRef] [PubMed]
118. Siebert, C.; Kramers, J.D.; Meisel, T.; Morel, P.; Nägler, T.F. PGE, Re-Os, and Mo isotope systematics in Archean and Early Proterozoic sedimentary systems as proxies for redox conditions on the early Earth. *Geochim. Cosmochim. Acta* **2005**, *69*, 1787–1812. [CrossRef]

119. Rye, R.; Holland, H.D. Paleosols and the evolution of the atmosphere: A critical review. *Am. J. Sci.* **1998**, *298*, 621–672. [CrossRef]
120. Klein, C.; Beukes, N.J. Geochemistry and sedimentology of a facies transition from limestone to iron-formation deposition in the Early Proterozoic Transvaal Supergroup, South Africa. *Econ. Geol.* **1989**, *84*, 1733–1774. [CrossRef]
121. Lascelles, D.F. Black smokers and density currents: A uniformitarian model for the genesis of banded iron-formations. *Ore Geol. Rev.* **2007**, *32*, 381–411. [CrossRef]
122. Prasad, J.; Venkatesh, A.S.; Sahoo, P.R. A submarine hydrothermal origin of banded iron formations from Archean Kiriburu-Meghahatuburu iron ore deposit, Singhbhum Craton, eastern India. *Ore Geol. Rev.* **2022**, *150*, 105125. [CrossRef]
123. Ohmoto, H. Non-redox transformations of magnetite-hematite in hydrothermal systems. *Econ. Geol.* **2003**, *98*, 157–161. [CrossRef]
124. Nutman, A.P.; McGregor, V.R.; Shiraishi, K.; Friend, C.; Bennett, V.; Kinny, P.D. 3850 Ma BIF and mafic inclusions in the early Archaean Itsaq Gneiss Complex around Akilia, southern West Greenland? The difficulties of precise dating of zircon-free protoliths in migmatites. *Precambrian Res.* **2002**, *117*, 185–224. [CrossRef]
125. Zhai, M.G.; Sills, J.D.; Windley, B.F. Metamorphic minerals and metamorphism of Anshan group in Anshan-Benxi area Liaoning. *Acta Petrol. Et Mineral.* **1990**, *9*, 148–158. (In Chinese with English abstract)
126. Planavsky, N.J.; McGoldrick, P.; Scott, C.T.; Li, C.; Reinhard, C.T.; Kelly, A.E.; Chu, X.L.; Bekker, A.; Love, G.D.; Lyons, T.W. Widespread iron-rich conditions in the Mid-Proterozoic ocean. *Nature* **2011**, *477*, 448–495. [CrossRef]
127. Poulton, S.W.; Canfield, D.E. Ferruginous conditions: A dominant feature of the ocean through Earth's history. *Elements* **2011**, *7*, 107–112. [CrossRef]
128. Reinhard, C.T.; Planavsky, N.J.; Robbins, L.J.; Partin, C.A.; Gill, B.C.; Lalonde, S.V.; Bekker, A.; Konhauser, K.O.; Lyons, T.W. Proterozoic ocean redox and biogeochemical stasis. *Proc. Natl. Acad. Sci. USA* **2013**, *110*, 5357–5362. [CrossRef]
129. Zhang, K.; Zhu, X.; Wood, R.A.; Shi, Y.; Gao, Z.; Poulton, S.W. Oxygenation of the Mesoproterozoic ocean and the evolution of complex eukaryotes. *Nat. Geosci.* **2018**, *11*, 345–350. [CrossRef]
130. Shang, M.; Tang, D.; Shi, X.; Zhou, L.; Zhou, X.; Song, H.; Jiang, G. A pulse of oxygen increase in the Early Mesoproterozoic ocean at ca. 1.57~1.56 Ga. *Earth Planet. Sci. Lett.* **2019**, *527*, 115797. [CrossRef]
131. Porter, S.M. Insights into eukaryogenesis from the fossil record. *Interface Focus* **2020**, *10*, 20190105. [CrossRef]
132. Planavsky, N.J.; Slack, J.F.; Cannon, W.F.; O'Connell, B.; Isson, T.T.; Asael, D.; Jackson, J.C.; Hardisty, D.S.; Lyons, T.W.; Bekker, A. Evidence for episodic oxygenation in a weakly redox-buffered deep mid-proterozoic ocean. *Chem. Geol.* **2018**, *483*, 581–594. [CrossRef]
133. Slack, J.F.; Grenne, T.; Bekker, A.; Rouxel, O.J.; Lindberg, P.A. Suboxic deep seawater in the Late Paleoproterozoic: Evidence from hematitic chert and iron formation related to seafloor-hydrothermal sulfide deposits, central Arizona, USA. *Earth Planet. Sci. Lett.* **2007**, *255*, 243–256. [CrossRef]
134. Mhlanga, X.R.; Tsikos, H.; Lee, B.; Rouxel, O.J.; Boyce, A.C.; Harris, C.; Lyons, T.W. The Palaeoproterozoic Hotazel BIF-Mn Formation as an archive of Earth's earliest oxygenation. *Earth-Sci. Rev.* **2023**, *240*, 104389. [CrossRef]
135. Kirschvink, J.L.; Gaidos, E.J.; Bertani, L.E.; Beukes, N.J.; Gutzmer, J.; Maepa, L.N.; Steinberger, R.E. Paleoproterozoic snowball Earth: Extreme climatic and geochemical global change and its biological consequences. *Proc. Natl. Acad. Sci. USA* **2000**, *97*, 1400–1405. [CrossRef] [PubMed]
136. Johnson, J.E.; Webb, S.M.; Ma, C.; Fischer, W.W. Manganese mineralogy and diagenesis in the sedimentary rock record. Geochim. *Cosmochim. Acta* **2016**, *173*, 210–231. [CrossRef]
137. Kennedy, B.; Runnegar, A.R.; Prave, K.H.; Hoffmann, M.A. Two or four Neoproterozoic glaciations? *Geology* **1998**, *26*, 1059–1063. [CrossRef]
138. Young, G.M. Iron-formation and glaciogenic rocks of the Rapitan Group, Northwest Territories, Canada. *Precambrian Res.* **1976**, *3*, 137–158. [CrossRef]
139. El-Rahman, Y.A.; Gutzmer, J.; Li, X.; Seifert, T.; Li, C.; Ling, X.; Li, J. Not all Neoproterozoic iron formations are glaciogenic: Sturtian-aged non-Rapitan exhalative iron formations from the Arabian-Nubian Shield. *Miner. Depos.* **2020**, *55*, 577–596. [CrossRef]
140. Xu, D.R.; Wang, Z.L.; Cai, J.X.; Wu, C.; Bakun-Czubarow, N.; Wang, L.; Chen, H.; Baker, M.J.; Kusiak, M.A. Geological characteristics and metallogenesis of the Shilu Fe-ore deposit in Hainan Province, South China. *Ore Geol. Rev.* **2013**, *53*, 318–342. [CrossRef]
141. Xu, D.R.; Wang, Z.L.; Chen, H.Y.; Hollings, P.; Jansen, N.H.; Zhang, Z.C.; Wu, C.J. Petrography and geochemistry of the Shilu Fe-Co Cu ore district, South China: Implications for the origin of a Neoproterozoic BIF system. *Ore Geol. Rev.* **2014**, *57*, 322–350. [CrossRef]
142. Sun, J.; Zhu, X.K.; Li, Z.H. Confirmation and global significance of a large-scale Early Neoproterozoic banded iron formation on Hainan Island, China. *Precambrian Res.* **2018**, *307*, 82–92. [CrossRef]
143. Lei, R.X.; Wu, C.Z.; Feng, Y.G.; Xia, M.Z.; Jian, J.G. Formation age and geodynamic setting of the Neoproterozoic Shalong iron formation in the Central Tianshan, NW China: Constraints from zircon U-Pb dating, geochemistry, and Hf-Nd isotopes of the host rocks. *Geol. J.* **2018**, *53*, 345–361. [CrossRef]
144. Stern, R.J.; Mukherjee, S.K.; Miller, N.R.; Ali, K.; Johnson, P.R. ~750 Ma banded iron formation from the Arabian-Nubian shield implications for understanding Neoproterozoic tectonics, volcanism, and climate change. *Precambrian Res.* **2013**, *239*, 79–94. [CrossRef]

145. Gao, B.F.; Wu, C.Z.; Li, W.Q.; Yang, T.; Ye, H.; Lei, R.X.; Liu, Q. Oxidation and deposition of iron-rich saline water below glacier cap: Genesis of Neoproterozoic Quruqsay iron deposit on northern margin of Tarim craton. *Miner. Depos.* **2018**, *37*, 1–26. (In Chinese with English abstract)
146. Gao, B.F.; Wu, C.Z.; Yang, T.M.; Santosh, M.; Dong, L.H.; Zhao, T.Y.; Ye, H.; Lei, R.X.; Li, W. The Neoproterozoic "Blood falls" in Tarim Craton and their possible connection with Snowball Earth. *J. Geophys. Res. Earth Surf.* **2019**, *124*, 229–244. [CrossRef]
147. Basta, F.F.; Maurice, A.E.; Fontboté, L.; Favarger, P.Y. Petrology and geochemistry of the banded iron formation (BIF) of WadiKarim and Um Anab, eastern Desert, Egypt: Implications for the origin of Neoproterozoic BIF. *Precambrian Res.* **2011**, *187*, 277–292. [CrossRef]
148. Freitas, B.T.; Warren, L.V.; Boggiani, P.C.; Almeida, R.P.D.; Piacentini, T. Tectono-sedimentary evolution of the Neoproterozoic BIF-bearing Jacadigo Group, SW-Brazil. *Sediment. Geol.* **2011**, *238*, 48–70. [CrossRef]
149. Berner, R.A. Atmospheric oxygen over Phanerozoic time. *Proc. Natl. Acad. Sci. USA* **1999**, *96*, 10955–10957. [CrossRef]
150. Lenton, T.M.; Dahl, T.W.; Daines, S.J.; Mills, B.J.; Ozaki, K.; Saltzman, M.R.; Porada, P. Earliest land plants created modern levels of atmospheric oxygen. *Proc. Natl. Acad. Sci. USA* **2016**, *113*, 9704–9709. [CrossRef]
151. Wallace, M.W.; Hood, A.V.; Shuster, A.; Greig, A.; Planavsky, N.J.; Reed, C.P. Oxygenation history of the Neoproterozoic to Early Phanerozoic and the rise of land plants. *Earth Planet. Sci. Lett.* **2017**, *466*, 12–19. [CrossRef]
152. Krause, A.J.; Mills, B.J.; Zhang, S.; Planavsky, N.J.; Lenton, T.M.; Poulton, S.W. Stepwise oxygenation of the Paleozoic atmosphere. *Nat. Commun.* **2018**, *9*, 4081. [CrossRef]
153. Clarkson, M.O.; Wood, R.A.; Poulton, S.W.; Richoz, S.; Newton, R.J.; Kasemann, S.A.; Bowyer, F.; Krystyn, L. Dynamic anoxic ferruginous conditions during the end-Permian mass extinction and recovery. *Nat. Commun.* **2016**, *7*, 12236. [CrossRef]
154. Song, H.; Jiang, G.; Poulton, S.W.; Wignall, P.B.; Wang, C. The onset of widespread marine red beds and the evolution of ferruginous oceans. *Nat. Commun.* **2017**, *8*, 399. [CrossRef] [PubMed]
155. Ramanaidou, E.R.; Wells, M.A. Sedimentary hosted iron ores. *Treatise Geochem.* **2014**, 313–355.
156. Flick, H.; Nerbor, H.D.; Heidelberg, R.B. Iron ore of the LahnDill type formed by diagenetic seeping of pyroclastic sequences-a case study on the Schalstein section at Gäinsberg (Weilburg). *Geol. Rundscchau* **1990**, *79*, 401–415. [CrossRef]
157. Yang, X.Q.; Mao, J.W.; Jiang, Z.S.; Santosh, M.; Zhang, Z.H.; Duan, S.G.; Wang, D.C. The carboniferous Shikebutai iron deposit in Western Tianshan, northwestern China: Petrology, Fe-O-C-Si isotopes, and implications for iron pathways. *Econ. Geol.* **2019**, *114*, 1207–1222. [CrossRef]
158. Klatt, J.M.; Chennu, A.B.; Arbic, K.B.; Biddanda, A.J.; Dick, G. Possible link between Earth's rotation rate and oxygenation. *Nat. Geosci.* **2021**, *14*, 564. [CrossRef]
159. Knoll, A.H. The geological consequences of evolution. *Geobiology* **2003**, *1*, 3–14. [CrossRef]
160. Knoll, A.H.; Javaux, E.J.; Hewitt, D.; Cohen, P. Eukaryotic organisms in Proterozoic oceans. *Philos. Trans. R. Soc. Biol. Sci.* **2006**, *361*, 1023–1038. [CrossRef]
161. Moczydlowska, M. The Ediacaran microbiota and the survival of Snowball Earth conditions. *Precambrian Res.* **2008**, *167*, 1–15. [CrossRef]
162. Walcott, C.D. Precambrian fossiliferous formations. *Bull. Geol. Soc. Am.* **1899**, *10*, 199–204. [CrossRef]
163. Sprigg, R.C. Early Cambrian (?) jellyfishes from the Flinders ranges, South Australia. *Trans. R. Soc. South Aust.* **1947**, *71 (Pt. 2)*, 212–224.
164. McMenamin, M.A.S.; McMenamin, D.L.S. *The Emergence of Animals: The Cambrian Breakthrough*; Columbia University Press: New York, NY, USA, 1990; p. 217.
165. Peterson, K.J.; McPeek, M.A.; Evans, D.A.D. Tempo and mode of early animal evolution: Inferences from rocks, Hox, and molecular clocks. *Paleobiology* **2005**, *31* (Suppl. 2), 36–55. [CrossRef]
166. Knoll, A.H. Learning to tell Neoproterozoic time. *Precambrian Res.* **2000**, *100*, 3–20. [CrossRef]
167. Narbonne, G.M.; Kaufman, A.J.; Knoll, A.H. Integrated chemostratigraphy and biostratigraphy of the Windermere Supergroup, northwestern Canada: Implications for Neoproterozoic correlations and the early evolution of animals. *Geol. Soc. Am. Bull.* **1994**, *106*, 1281–1292. [CrossRef]
168. Erwin, D.H. Dates and rates: Temporal resolution in the deep time stratigraphic record. *Annu. Rev. Earth Planet. Sci.* **2006**, *34*, 569–590. [CrossRef]
169. Marshall, C.R. Explaining the Cambrian "Explosion" of Animals. *Annu. Rev. Earth Planet. Sci.* **2006**, *34*, 355–384. [CrossRef]
170. McCall, G.J.H. The Vendian (Ediacaran) in the geological record: Enigmas in geology's prelude to the Cambrian explosion. *Earth-Sci. Rev.* **2006**, *77*, 1–229. [CrossRef]
171. Meert, J.G.; Lieberman, B.S. The Neoproterozoic assembly of Gondwana and its relationship to the Ediacaran–Cambrian radiation. *Gondwana Res.* **2008**, *14*, 5–21. [CrossRef]
172. Payne, J.L.; Boyer, A.G.; Brown, J.H.; Finnegan, S.; Kowalewski, M.; Krause, R.A., Jr.; Lyons, S.K.; McClain, C.R.; McShea, D.W.; Novack-Gottshall, P.M.; et al. Two-phase increase in the maximum size of life over 3.5 billion years reflects biological innovation and environmental opportunity. *Proc. Natl. Acad. Sci.* **2009**, *106*, 24. [CrossRef]
173. Wang, C.L.; Konhauser, K.O.; Zhang, L.C. Depositional environment of the Paleoproterozoic Yuanjiacun banded iron formation in Shanxi Province, China. *Econ. Geol.* **2015**, *110*, 1515–1539. [CrossRef]
174. Condie, K.C. Episodic continental growth and supercontinents: A mantle avalanche connection? *Earth Planet. Sci. Lett.* **1998**, *163*, 97–108. [CrossRef]

175. Condie, K.C. Continental growth during a 1.9-Ga superplume event. *J. Geodyn.* **2002**, *34*, 249–264. [CrossRef]
176. Franklin, J.M.; Gibson, H.L.; Jonasson, I.R.; Galley, A.G. Volcanogenic massive sulfide deposits. *Econ. Geol.* **2005**, *100*, 523–560.
177. Meert, L.M.; Peck, D.; Toope, K. Timing and geochemistry of 1.88 Ga Molson Igneous Events, Manitoba: Insights into the formation of a craton-scale magmatic and metallogenic province. *Precambr. Res.* **2009**, *172*, 143–162.
178. Meert, J.G.; Pandit, M.K.; Pradhan, V.R.; Kamenov, G. Preliminary report on the paleomagnetism of 1.88 Ga dykes from the Bastar and Dharwar cratons, peninsular India. *Gondwana Res.* **2011**, *20*, 335–343. [CrossRef]
179. Blum, N.; Crocker, J.H. Repetitive cyclical volcanism in the Late Archean Larder Lake Group near Kirkland Lake, Ontario: Implications of geochemistry on magma genesis. *Precambrian Res.* **1992**, *54*, 173–194. [CrossRef]
180. Jackson, S.L.; Fyon, J.A.; Corfu, F. Review of Archean supracrustal assemblages of the southern Abitibi greenstone belt in Ontario, Canada: Products of microplate interaction within a large-scale plate-tectonic setting. *Precambrian Res.* **1994**, *65*, 183–205. [CrossRef]
181. Stevenson, R. Crust and mantle evolution in the Late Archean: Evidence from a Sm-Nd studyof the North Spirit Lake Greenstone Belt, northwestern Ontario, Canada, Geol. Soc. *Am. Bull.* **1995**, *107*, 1458–1467. [CrossRef]
182. Thurston, P.C.; Ayer, J.A.; Goutier, J. Depositional Gaps in Abitibi Greenstone Belt Stratigraphy: A Key to Exploration for Syngenetic Mineralization. *Econ. Geol.* **2008**, *103*, 1097–1134. [CrossRef]
183. Veizer, J.; Laznicka, P.; Jansen, S.L. Mineralization through Geologic Time; Recycling Perspective. *Am. J. Sci.* **1989**, *289*, 484–524. [CrossRef]
184. Huston, D.L.; Champion, D.C.; Cassidy, K.F. Tectonic Controls on the Endowment of Neoarchean Cratons in Volcanic-Hosted Massive Sulfide Deposits: Evidence from Lead and Neodymium Isotopes. *Econ. Geol.* **2014**, *109*, 11–26. [CrossRef]
185. Dreher, A.M.; Xavier, R.P.; Taylor, B.E. New Geologic, Fluid Inclusion and Stable Isotope Studies on the Controversial Igarapé Bahia Cu-Au Deposit, Carajás Province, Brazil. *Miner. Depos.* **2008**, *43*, 161–184. [CrossRef]
186. Qi, S.J.; Wang, C.Y.; Yang, J.P. The Origin of the Precambrian Metavolcanic-Sedimentary Rock Systems and the Massive Sulfide Deposits in Xingshutai Neiqiu, Hebei Province. *J. Hebei Coll. Geol.* **1983**, *22*, 1–16. (In Chinese)
187. Zhu, M.T.; Zhang, L.C.; Dai, Y.P. In Situ Zircon U-Pb Dating and O Isotopes of the Neoarchean Hongtoushan VMS Cu-Zn Deposit in the North China Craton: Implication for the Ore Genesis. *Ore Geol. Rev.* **2019**, *67*, 354–367. [CrossRef]
188. Peng, Z.D.; Wang, C.L.; Zhang, L.C. Geochemistry of Metamorphosed Volcanic Rocks in the Neoarchean Qingyuan Greenstone Belt, North China Craton: Implications for Geodynamic Evolution and VMS Mineralization. *Precambrian Res.* **2017**, *326*, 196–221. [CrossRef]
189. DeWit, M.J.; Roering, C.R.; Hart, J.; Armstrong, R.A.; de Ronde, C.E.J.; Green, R.W.E.; Tredoux, M.; Peberdy, E.; Hart, R.A. Formation of an Archean continent. *Nature* **1992**, *357*, 553–562. [CrossRef]
190. Card, K.D. A review of the Superior Province of the Canadian Shield, a product of Archean accretion. *Precambrian Res.* **1990**, *48*, 99–156. [CrossRef]
191. Malinowski, M.; White, D.J.; Mwenifumbo, C.J. Seismic Exploration for VMS Deposits within the Paleoproterozoic Flin Flon Belt, Trans-Hudson Orogen, Canada. *Geophys. Res.* **2008**, *10*, 37–45.
192. Schneider, D.A.; Bickford, M.E.; Cannon, W.F. Age of Volcanic Rocks and Syndepositional Iron Formations, Marquette Range Supergroup: Implications for the Tectonic Setting of Paleoproterozoic Iron Formations of the Lake Superior Region. *Can. J. Earth Sci.* **2002**, *39*, 999–1012. [CrossRef]